Results in Earth Sciences 3 (2025) 100070

Contents lists available at ScienceDirect

Results in Earth Sciences

journal homepage: www.sciencedirect.com/journal/results-in-earth-sciences

Petrogenesis, geodynamic setting, age of Rhyacian igneous rocks, from Nampala gold deposit: Implications for the crustal growth of the Birimian terrain in southern Mali

Sory I.M. Konate [a,*], Mamadou L. Bouare [b], Anthony T. Bolarinwa [c], Daniel Kwayisi [d,e], Raymond Webrah Kazapoe [f], Elhadji Mory Traore [a], N.'Tcha Daniel Kouagou N'Dah [a]

[a] Pan African University Life and Earth Sciences Institute (PAULESI), University of Ibadan, Ibadan, Nigeria
[b] Ecole Nationale d'Ingénieurs Abderhamane Baba Touré, Bamako, Mali
[c] Department of Geology, University of Ibadan, Ibadan, Nigeria
[d] University of Johannesburg, Department of Geology, Auckland Park Kingsway Campus, Johannesburg, South Africa
[e] University of Ghana, Department of Earth Science, Legon-Accra, Ghana
[f] Department of Geological Engineering, University for Development Studies, Nyankpala, Ghana

ARTICLE INFO

Keywords:
Geochemistry, zircon Geochronology
Hf isotopes
Crustal growth, South Mali

ABSTRACT

The Nampala gold deposit is a sub-world-class deposit situated within the Birimian terrain of southern Mali, it is characterized by metasedimentary, intrusive, and graphitic schist rocks. This study investigated the petrography, geochemistry, and geochronology of the intrusive rocks (lamprophyre and granitoid) to elucidate their origins, petrogenesis, age, and tectonic settings. The lamprophyres are porphyritic and holocrystalline and are composed of pyroxene and amphibole, some of the mafic minerals have been altered to talc. The granitoids are coarse-grained and composed predominantly of plagioclase, with minor quartz, microcline, biotite, and sulfides. The lamprophyres exhibit subalkaline, specifically calc-alkaline characteristics, enrichment of Light Rare Earth Elements (LREE) to Heavy Rare Earth Elements (HREE), intermediate ratios of Dy/Yb and Sm/Yb between 1.8 – 2.0 and 2.5 – 2.9, respectively, high Rb/Sr (0.56 – 0.79), and low Ba/Rb (2.04 – 2.50) ratios. These features indicate formation through low-degree partial melting of phlogopite-bearing lherzolite in the spinel-garnet transition zone at depths of 75–80 km. The granitoids are granodiorite and crystallized at 2.1 Ga, I-type. They are peraluminous, and high-K calc-alkaline, with subchondritic εHf(t) values (-1.83–3.3) and TDM1 model ages (2.52 – 2.33 Ga). These signatures suggest a hybrid origin involving juvenile mantle melts and recycled Paleoproterozoic crust during an accretionary orogen. The Mg# and SiO_2 contents of the granitoids' along with REE patterns and Ba, Sr, and Eu anomalies, imply melting of the delaminated lower crust. Trace element patterns, and negative Nb, Ta, and Ti anomalies, support a subduction-related genesis for both rock types. The findings provide critical constraints on the subduction-accretion processes contributing to the evolution of the Birimian Terrain within the West African Craton.

Introduction

The Birimian terrain is regarded as a crucial region of crustal development through the Paleoproterozoic. The terrain consists of granitoid-greenstone belts and sedimentary basins (Sakyi et al., 2014; Anum et al., 2015; Agra et al., 2023). In Mali, the terrain is divided into western and southern parts. The Kédougou-Kéniéba Inlier (KKI) is the farthest west outcrop of the Birimian in the Leo-Man shield. It is distinct from most of the Palaeoproterozoic terrains due to the presence of Neoproterozoic sandstones from the Taoudeni Basin that overlie it. Lambert Smith et al. (2016) argued that the tectonic conditions in the KKI region transitioned from a volcanic island arc environment to an active continental margin. The process of crustal thickening, caused by a transition to a collisional tectonic environment, together with magmatic differentiation, resulted in the creation of peraluminous, granitic melts that incorporated a substantial amount of crustal material. On the eastern edge of the Dialé-Daléma basin, Lambert Smith et al. (2016) pointed out the presence of a small suite of more basic intrusive and

* Corresponding author.
E-mail address: sorymadykonate@yahoo.com (S.I.M. Konate).

https://doi.org/10.1016/j.rines.2025.100070
Received 23 November 2024; Received in revised form 2 February 2025; Accepted 3 February 2025
Available online 8 February 2025

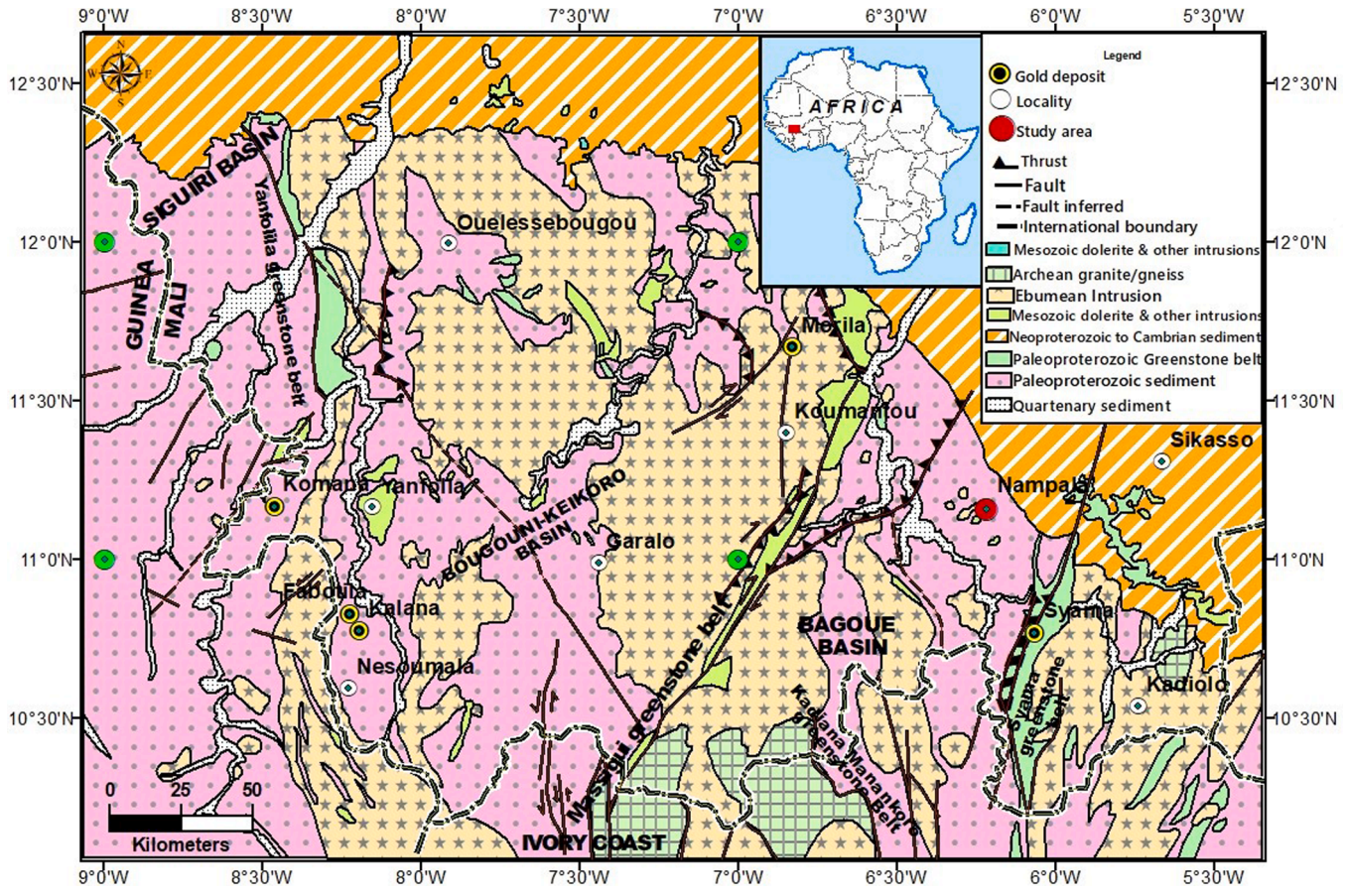

Fig. 1. Geological map of Southern Mali modified after Sangare (2015).

extrusive rocks. These rocks have a metaluminous composition and show a modest enrichment of large-ion lithophile elements (LILE). The Daléma igneous rocks likely originated in an extensional back-arc, which is connected to the arc system.

In southern Mali, there are limited outcrops of Paleoproterozoic formations and they are obscured by thick lateritic soils. In the Massigui region in southern Mali, Wane et al. (2018) proposed a regional tectonic model consisting of three main events: 1. Oceanic plate subduction towards the east below the Baoulé-Mossi Birimian segment, occurring around 2.125 Ga ago. 2. Oblique continental subduction of the Archean Kenema-Man craton, taking place between 2.125 and 2.090 Ga ago. This event led to the closure of the Birimian Ocean (collision stage). It also involved significant movements along the Banifing shear zone, as well as magmatism and volcano-sedimentary deposition in the Massigui region. 3. Metacratonization of the subducting Kenema-Man craton, occurring between 2.09 and 2.02 Ga ago. This event resulted in the emplacement of magmas derived from Archean protoliths, which is a key difference compared to the Baoulé-Mossi juvenile granitoids. From paleomagnetic data, as well as the occurrence of similar lithologies and ages, it may be deduced that the Kenema-Man craton was once part of the Sarmatia craton. This relationship establishes a correlation between the geotectonic evolution of the area and the fusion of the Columbia supercontinent (Wane et al., 2018) Southern Mali possesses a significant number of gold deposits and is the second-largest gold belt in Mali. Gold mineralization is hosted by detrital sedimentary rocks, diorite (Salvi et al., 2015, Sangare, 2015), granodiorite, tonalite greywacke, volcanoclastic rock (Mcfarlane et al., 2011, Hammond et al., 2011), microgranite, volcano-sedimentary rocks, basalts, andesite, and pyroclastic conglomerates (Olson et al., 1992, Traore, 2017).

The Nampala gold deposit is situated in southern Mali within the Bagoé Basin; regionally, within the Birimian terrain of the Baoulé-Mossi Domain (Kerr-Gillespie et al., 2018). The deposit contains a thick sequence of greywacke, siltstone, and shale belonging to the Paleoproterozoic Birimian terrane (Kerr-Gillespie et al., 2018; Konate et al., 2024). These sequences have been intruded by several dykes and sills, including gabbro, lamprophyre, and granitoids. According to the latest findings by Konate et al. (2024), subduction-accretion processes produced Nampala's sedimentary rocks in a subduction-related environment. Gold mineralization at Nampala is associated with dense dissemination of fine-grained pyrite and arsenopyrite (Konate et al., 2024) within metasediments and granitoids and linked to stockworks of quartz and carbonate veins (Kerr-Gillespie et al., 2018). Although igneous rocks (specifically granitoid) and gold mineralization have a strong relationship within the Bagoe Basintheir tectonic context and petrogenesis are as yet unknown. Due to the lack of outcrops and thick lateritic and alluvial cover, we have conducted a petrographic study and analyzed the geochemical compositions of lamprophyres and granodiorite of the Nampala Gold deposit from diamond drill core.

This investigation is the first comprehensive geochemical investigation to examine the petrogenesis and tectonic setting of the lamprophyres and granodiorites from the Nampala Gold deposit. Zircon U-Pb and Lu-Hf isotope data are presented to point out the timing of the rocks' emplacement and the source of the magma

Geological setting

The southern part of Mali consists of Paleoproterozoic formations, which are only partially exposed within extensively developed lateritic formations. It is comprised of a series of greenstone belts that are aligned in a north-northeast direction and are split by sedimentary basins (Traore et al., 2022). According to Girard et al. (1998), there are three sedimentary basins from west to east, each associated with four

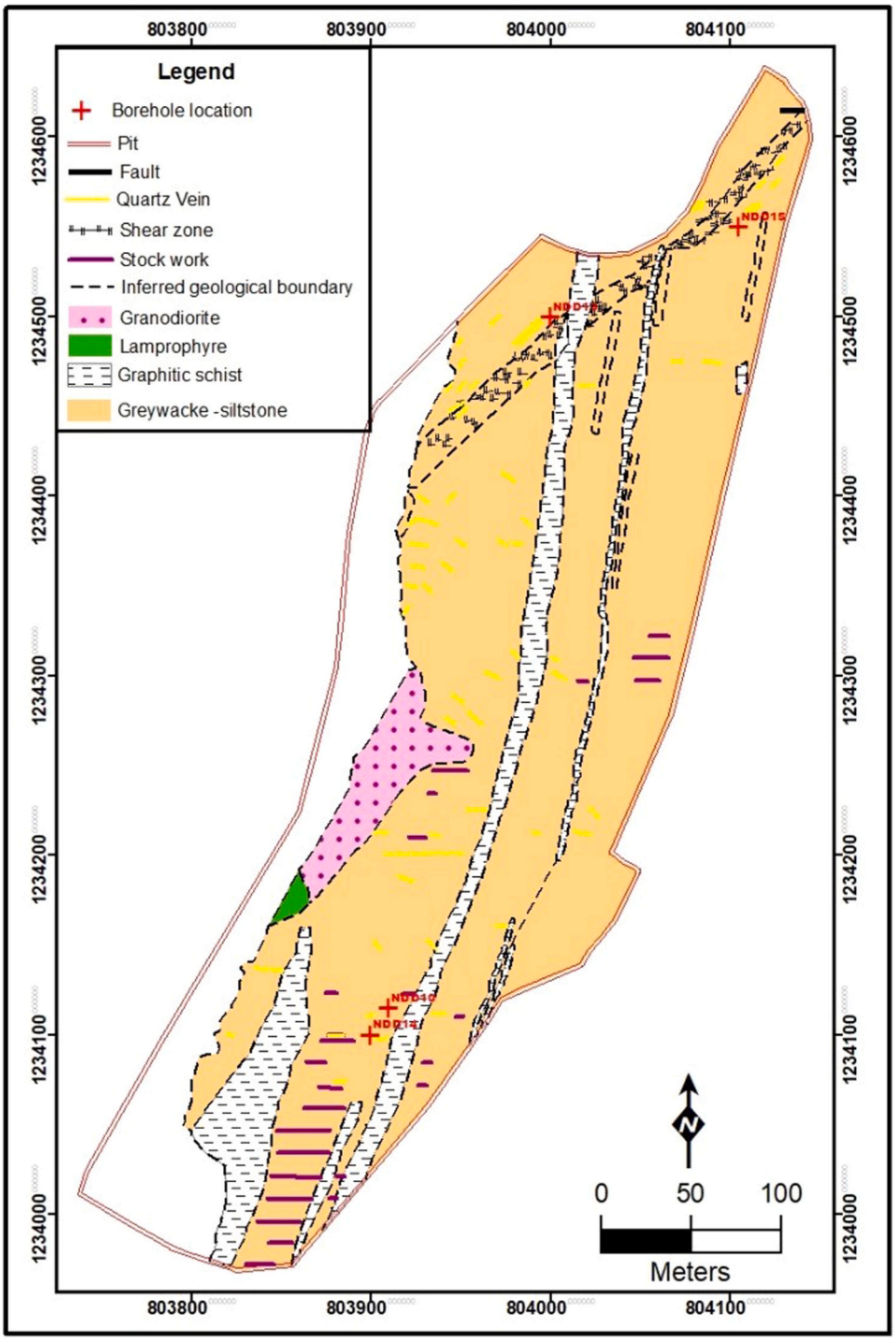

Fig. 2. Geological Map of Nampala gold deposit.

volcano-sedimentary belts (Fig. 1) The Siguiri basin which extends into Guinea and a small part of it crops out in Mali. It is bordered to the east by the Yanfolila volcano-plutonic belt, which extends southwards into Ivory Coast and Guinea. 2) The Bougouni-Kékoro basin, composed of scattered fragments enclosed within a large granitic batholitic complex, which marks the western boundary of the Bagoé basin. 3) The Bagoé basin, which is the most significant basin in southern Mali due to its gold resources. It is bordered by the sedimentary basin of the Kadiana-Madinani domain on the west and the sedimentary formations of the Kadiolo domain on the east. According to Kusnir and Diallo (1986), the volcano-sedimentary succession to the east is mildly metamorphosed. It is mostly composed of schists, metagreywackes, and meta-arkoses, whereas schists, metaquartzwackes/metagreywackes, and metavolcanic rocks, primarily with an intermediate composition are the three lithologies found to the west (Liégeois et al., 1991). The Tiékongoba-Niamala Series is a volcano-sedimentary series that lies at the northwest border of the Bagoé basin, west of the Bagoé River (Wane, 2010). The bulk of this series consists of felsic metavolcanic lavas intercalated with biotite muscovite quartzo feldspathic metasedimentary rocks.

The Bagoé Formation, located within the Bagoe Basin, extends northeast and stretches for many kilometers into Côte d'Ivoire,

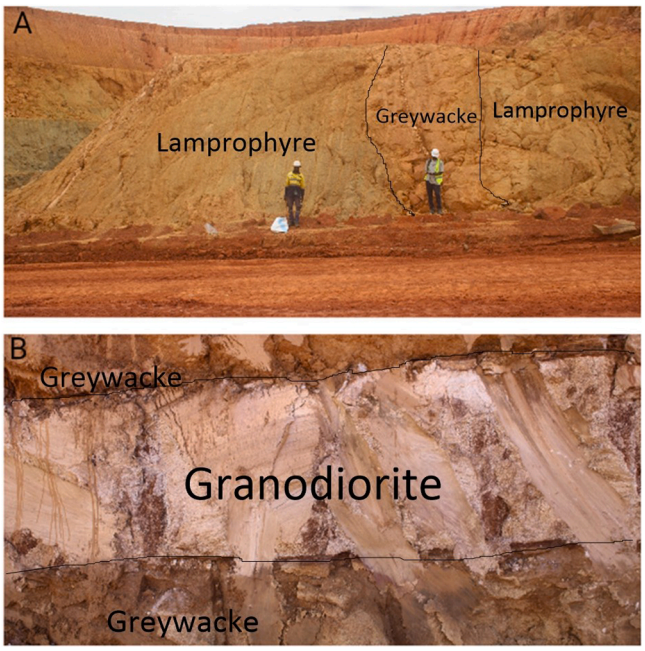

Fig. 3. Field photo taken within Nampala gold deposit showing the mode of occurrence of igneous and sedimentary rocks. A: Greywacke within 2 dykes of Lamprophyres; B: Granodiorite intruded within 2 layers of Greywacke.

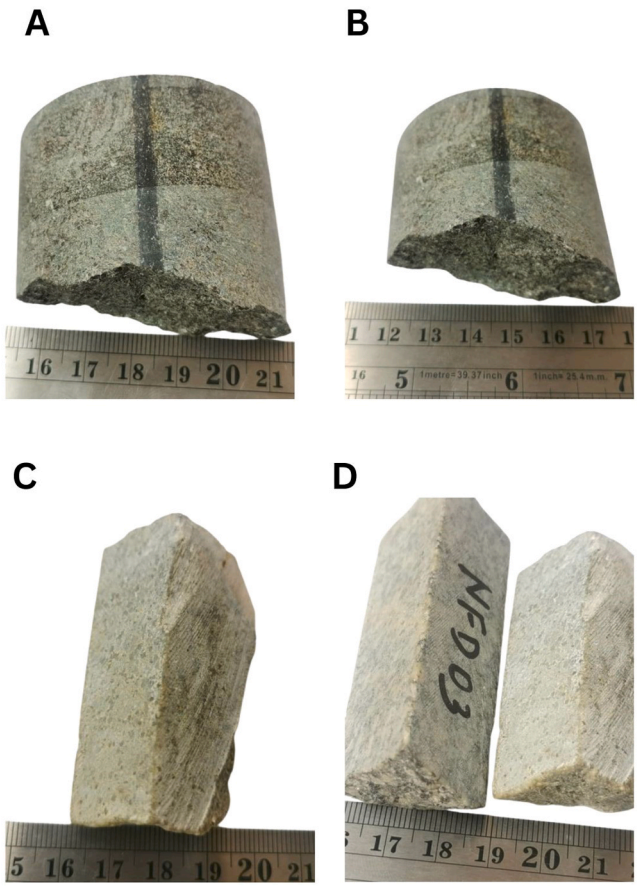

Fig. 4. Hand specimen of igneous rocks from Nampala gold deposit A-B: Lamprophyre and C-D: Granodiorite.

disappearing beneath the Taoudeni Basin to the north (Ballo et al., 2016). This formation primarily consists of turbidites, which have been intruded by gabbroic dykes and sills, late felsic dykes and sills, and substantial porphyritic intermediate stocks that penetrate the flysch sequences of the Bagoé Formation (Bentley et al., 2000; Traoré et al., 2019). These turbidites host the Nampala Gold deposit (Fig. 2), trend NNE dip steeply to the ESE (Kerr-Gillespie et al., 2018), and form thick sequences of interbedded shale, siltstone, and greywacke, sometimes referred to as mudstone, claystone, schist, phyllite, or argillite in mine terminology (Marchand, 2012; Kerr-Gillespie et al., 2018). A significant unit in this region is graphitic schist, which displays high MAG/IP conductivity on geophysical maps but is not anomalous in gold. The siliceous sandstones, or gritstones, consist of subrounded, coarse-grained lithic fragments of graphitic phyllite within a coarse-grained matrix of quartz and feldspar (Marchand, 2012; Kerr-Gillespie et al., 2018).

Throughout the deposit, extensive weathering is observed, affecting all lithologies down to depths of up to 100 m before transitioning to unweathered rock (Marchand, 2012; Kerr-Gillespie et al., 2018). The saprolite is covered by a thick layer of residual lateritic soil and duricrust, which can exceed 10 m in thickness. Due to the lateritic and alluvial cover, outcrops are rare. Consequently, detailed petrographic and geochemical studies were conducted to determine the provenance and tectonic setting of the siliciclastic sedimentary rocks of the Nampala Gold deposit from drill cores (Konate et al., 2024). The petrographic and geochemical characteristics of the siliciclastic rocks indicate that these rocks were formed in an active continental margin, similar to other sedimentary rocks of the Paleoproterozoic Birimian terrane (Konate et al., 2024). However, no documentation of the petrogenesis and tectonic setting of the intrusive igneous rocks has been recorded through petrographic and geochemical studies. Therefore, an assessment of the petrography and geochemistry of drill core samples is necessary to infer the petrogenesis and tectonic setting of the intrusive igneous rocks.

Sampling Procedure and Analytical Techniques

Rock sampling and Petrographic analysis

Because of the thick overburden in the study area, samples were obtained through diamond drilling from the Nampala Gold deposit. The drill core samples obtained comprise 5 lamprophyres and 5 granodiorites. A detailed examination of the thin sections was performed using a Leica DM 750 microscope at the Department of Geology, University of Ibadan, Nigeria.

Mineralogical analyses

An analysis was conducted on 8 typical samples from the Nampala gold deposit to determine their mineralogical composition. The samples consisted of 4 granodiorites and 4 lamprophyres. The analysis was performed using a PANalytical Empyrean x-ray Diffractometer at the University of Free State in South Africa. Detailed information on the methodology can be found in the supplementary file

Geochemical analyses

Ten fresh drill core samples, consisting of 5 lamprophyres and 5 granodiorites, were analyzed to assess their geochemical composition. The core samples were crushed to less than 2 mm and to 75 μm for further analysis at the Department of Geology, Obafemi Awolowo University, Ile-Ife, Nigeria, Analytical facility. The pulverised samples were then sent to the Activation Laboratory in Ontario, Canada, to analyze major oxides and trace elements concentrations. The concentrations of major oxides were examined using Inductively Coupled Plasma Optical Emission Spectroscopy (ICP-OES) method with the code 4 Lithoresearch analytical package, which detected limits ranging between 0.001 –

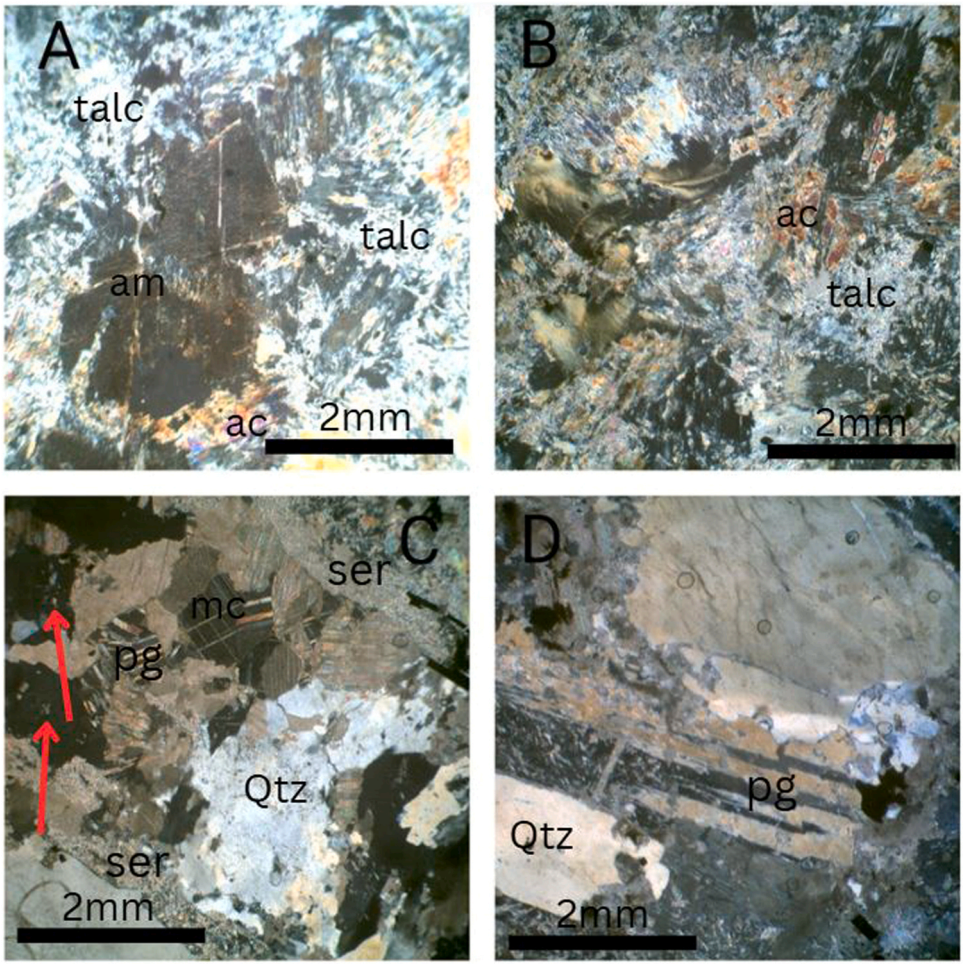

Fig. 5. Photomicrograph of igneous rocks, A-B =Lamprophyre and C-D= Granodiorite. Lamprophyre are foliated and dominated by altered minerals, Am: amphibole, ac: actinolite; mc: microcline, pg: plagioclase, ser: sericite, the red arrows in C are myrmekite.

0.01 %. The analysis of trace elements was conducted using Inductively Coupled Plasma Mass Spectrometry (ICP-MS) technique, with detection limits in the range of 0.005–30 ppm.

Zircon U-Pb and Lu-Hf analyses

A granodiorite core sample was crushed using the sledgehammer and sieved to below 250 μm at the Department of Geology, University of Johannesburg. The sieved sample was pan-washed to extract heavy minerals, such as zircon. Subsequently, the zircon were handpicked under a binocular microscope and mounted in an epoxy consisting of 4 g of Epoflex resin and 0.5 g of Epoflex hardener. Following this, the mount was polished to expose the zircon surfaces and imaged by cathodoluminescence (CL) in a Tescan-Vega 3 SEM at the Spectrum Analytical Facility, University of Johannesburg. The U-Pb age calculations only accepted ages with discordance between −10 % and + 10 % to minimize errors, while Pb-loss corrected zircons with low $^{204}Pb/^{206}Pb$ ratios were rejected (Agangi et al., 2018).

The same grains that were used for U-Pb dating were also analyzed for their Hf isotopic compositions. The ablation place used for the Hf isotope analysis was positioned in the exact same location as the prior spot used for U-Pb analysis. A software tool, available at https://github.com/magnuskristoffersen/detzrcr, was used to provide the U-Pb age and Lu-Hf isotope content using the approach described by Andersen et al. (2018). The methodology used for U-Pb and Lu-Hf isotope analysis are described in the Supplementary file.

RESULTS

Field Occurrence and Petrography

Fig. 3 displays a field photo illustrating the relation between igneous and sedimentary rock groups. It shows a sediment rock (greywacke) within 2 dykes of lamprophyres. Fig. 4 exhibits hand specimens collected for petrographic and geochemical investigations.

Lamprophyre is greenish-grey and has porphyritic and holocrystalline textures (Fig. 5(a,b)). It is foliated and dominated by altered minerals. These minerals include pyroxene and amphibole. The ferromagnesian minerals are significantly altered into talc, chlorite, indicating greenschist metamorphism grade and opaque minerals, however, with preserved pseudomorphs.

The granodiorites are grey, coarse-grained, massive, and granular (Fig. 5(c,d)). They are composed dominantly of plagioclase, with minor quartz, microcline, biotite and sulfides. Plagioclase may show slight alteration into sericite and calcite. The quartz shows undulose extinctions. Biotite is altered to chlorite and appears as overgrowth on the plagioclase. Calcite infiltration/impregnation is observed.

Mineralogy

Because all primary minerals have been altered into secondary minerals XRD analysis has been performed. Tables 4 and 5 show the modal composition of the studied rocks. Results from the XRD show that the granodiorites are composed of moderate quartz (25–28 %), mica

Table 1
Major oxides and trace elements composition for the Nampala Gold deposit lamprophyres and granodiorites.

	NFC01	NFC02	NFC03	NFC04	NFC05	NFD01	NFD02	NFD03	NFD04	NFD05
	Lamprophyres					Granodiorites				
SiO_2	46.8	45.83	44.21	45.71	46.23	59.08	59.58	65.62	59.36	72.5
TiO_2	0.377	0.477	0.457	0.451	0.462	0.416	0.417	0.351	0.507	0.264
Al_2O_3	8.58	8.08	7.42	8.25	7.71	16.07	15.54	14.16	16.08	10.88
Fe_2O_3(T)	11.27	11.48	11.16	11.55	11.29	3.9	4.38	3.36	5.13	2.77
MnO	0.146	0.146	0.167	0.143	0.142	0.062	0.057	0.05	0.075	0.041
MgO	19.84	19.48	18.66	19.72	19.39	2.08	1.95	1.66	2.66	1.28
CaO	5.42	5.6	7.24	5.12	5.55	3.78	3.4	3.09	3.3	2.52
Na_2O	0.22	0.16	0.19	0.17	0.18	3.41	2.49	3.39	4.17	2.86
K_2O	2.33	2.44	2.02	2.27	2.28	3.14	3.49	2.55	2.23	1.94
P_2O_5	0.19	0.19	0.2	0.2	0.2	0.27	0.35	0.26	0.39	0.22
LOI	5.21	5.16	6.39	4.96	4.75	6.6	7.12	5.54	5.39	4.34
Total	100.4	99.05	98.13	98.55	98.18	98.81	98.78	100	99.29	99.62
Mg#	77.72	77.08	76.81	77.18	77.29	51.38	46.87	49.47	50.68	47.80
Trace elements										
Sc	20	20	20	19	21	7	7	6	8	4
V	120	130	127	129	134	35	34	29	42	22
Cr	2280	2260	2320	2460	2320	50	50	40	50	30
Co	75	98	76	76	150	23	30	34	33	45
Ni	750	720	760	770	730	20	20	10	30	10
Cu	60	90	80	80	90	50	60	50	60	40
Zn	90	90	80	90	90	50	50	50	60	40
Ga	12	11	11	11	11	21	20	18	22	14
Rb	103	108	98	106	107	107	122	88	82	66
Sr	149	167	175	134	149	688	460	571	710	454
Y	9.3	10.4	12.9	9.4	10.6	10.1	10.4	8.7	11.6	6.7
Zr	61	65	68	56	67	168	169	138	200	100
Nb	2	2.4	2.5	2.1	2.5	5.9	5.7	4.5	7.1	3.3
Cs	12.3	12.3	12	13	12.4	3.8	3.7	2	3.4	1.6
Ba	210	270	238	243	249	695	594	545	687	422
Hf	1.5	1.5	1.6	1.4	1.7	3.4	3.6	2.9	4.4	2
Ta	0.19	0.54	0.23	0.19	1.27	0.61	0.66	0.7	0.76	0.62
Pb	< 5	< 5	< 5	< 5	< 5	6	6	24	12	39
Th	1.49	1.67	1.82	1.44	1.72	4.41	4.75	3.97	5.67	2.54
U	0.57	0.6	0.64	0.52	0.64	1.24	1.11	1.09	1.29	0.81
La	10.6	11	11.8	10.2	11.3	28.5	31.3	25.1	35.5	16.1
Ce	22.7	23.1	25.2	21.4	24.3	51.4	56.6	45.4	64.8	29.1
Pr	2.85	2.92	3.33	2.76	3.09	5.65	6.14	4.94	7.13	3.18
Nd	11.6	12.4	13.1	10.8	13	20	20.8	17.5	24.7	11.3
Sm	2.43	2.66	2.92	2.54	2.67	3.36	3.48	2.96	4.1	1.89
Eu	0.598	0.748	0.772	0.633	0.736	0.98	1.11	0.898	1.2	0.813
Gd	2.21	2.32	2.83	2.28	2.53	2.43	2.61	2.08	3.07	1.57
Tb	0.32	0.34	0.39	0.31	0.36	0.32	0.35	0.28	0.42	0.22
Dy	1.7	1.95	2.14	1.79	1.99	1.88	1.9	1.47	2.16	1.17
Ho	0.34	0.4	0.42	0.35	0.39	0.34	0.38	0.29	0.42	0.22
Er	1	1.06	1.22	0.95	1.12	0.93	1.1	0.84	1.21	0.63
Tm	0.133	0.152	0.177	0.139	0.157	0.138	0.156	0.124	0.172	0.088
Yb	0.87	1.05	1.19	0.89	1.04	0.98	0.95	0.86	1.19	0.6
Lu	0.131	0.165	0.184	0.137	0.158	0.158	0.148	0.14	0.188	0.097
Nb/Y	0.22	0.23	0.19	0.22	0.24	0.58	0.55	0.52	0.61	0.49
Zr/Ti	0.03	0.02	0.02	0.02	0.02	0.07	0.07	0.07	0.07	0.06
Ce/Yb	26.09	22.00	21.18	24.04	23.37	52.45	59.58	52.79	54.45	48.50
Th/Ce	0.07	0.07	0.07	0.07	0.07	0.09	0.08	0.09	0.09	0.09
Th/La	0.14	0.15	0.15	0.14	0.15	0.15	0.15	0.16	0.16	0.16
Lu/Yb	0.15	0.16	0.15	0.15	0.15	0.16	0.16	0.16	0.16	0.16
Rb/Sr	0.69	0.65	0.56	0.79	0.72	0.16	0.27	0.15	0.12	0.15
Ta/Yb	0.22	0.51	0.19	0.21	1.22	0.62	0.69	0.81	0.64	1.03
Th/Yb	1.71	1.59	1.53	1.62	1.65	4.50	5.00	4.62	4.76	4.23
Nb/U	3.51	4.00	3.91	4.04	3.91	4.76	5.14	4.13	5.50	4.07
Ba/Rb	2.04	2.50	2.43	2.29	2.33	6.50	4.87	6.19	8.38	6.39
La/Nb	5.30	4.58	4.72	4.86	4.52	4.83	5.49	5.58	5.00	4.88
Ba/Nb	105.00	112.50	95.20	115.71	99.60	117.80	104.21	121.11	96.76	127.88
Dy/Yb	1.95	1.86	1.80	2.01	1.91	1.92	2.00	1.71	1.82	1.95
Nb/Ta	10.53	4.44	10.87	11.05	1.97	9.67	8.64	6.43	9.34	5.32
Zr/Hf	40.67	43.33	42.50	40.00	39.41	49.41	46.94	47.59	45.45	50.00
Zr/Nb	30.50	27.08	27.20	26.67	26.80	28.47	29.65	30.67	28.17	30.30
Nb/Yb	2.30	2.29	2.10	2.36	2.40	6.02	6.00	5.23	5.97	5.50

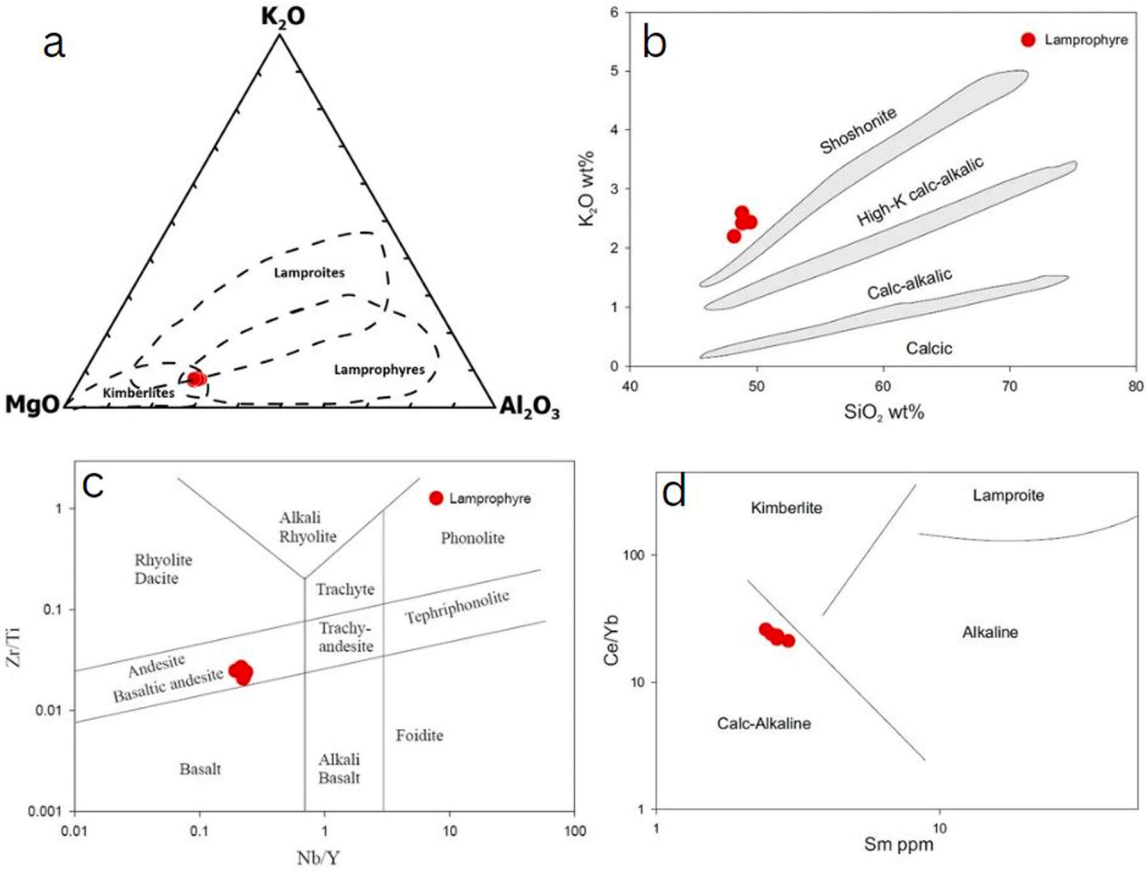

Fig. 6. Classification and magma characteristics of lamprophyres (a) MgO-K_2O-Al_2O_3 plot (after Bergmann, 1987), (b) K_2O vs SiO_2 plot, (c) Nb/Y vs Zr/Ti diagram (after Pearce, 1996), and (d) Sm vs Ce/Yb diagram (after Rock, 1991).

(15–23 %), and microcline (4–5 %) contents. Other mineral grains include plagioclase (22–25 %), dolomite (12–17 %), Kaolinite (3–6 %), clinochlore (10–12 %), and Opaque mineral (4–6 %). One sample recorded K-feldspar (5 %), and another recorded diopside (5 %).

The lamprophyres, on the other hand, recorded low quartz content (6–8 %), and subordinate calcite (6–12 %), amphibole (12–13 %), opaque mineral (4–6 %), and moderate clinochlore (21–23 %), mica (17–20 %), and talc (26–27 %). Representative diffractograms and modal compositions of the studied rocks are presented in the supplementary file.

Whole rock geochemistry

Major and trace elements characteristics

The major and trace element concentrations of the igneous rocks from the Nampala deposit are presented in Table 1. The lamprophyres have low SiO_2 content of 44.2 – 46.8 wt%, TiO_2 of 0.38 – 0.48 wt%, Al_2O_3 of 7.4 – 8.6 wt% and Na_2O of 0.16 – 0.22 wt%. However, they have high ferromagnesian oxide contents with $Fe_2O_{3\,t}$ of 11.2 – 11.6 wt % and MgO of 18.7 – 19.8 wt%. CaO contents of the lamprophyres are in the range of 5.1 – 7.2 wt%. LOI contents of the lamprophyres are high, ranging from 4.8 – 6.4 wt%. The low SiO_2 and high Fe_2O_3t and MgO contents correspond to a high Mg# of 77 – 78. In terms of trace elements, the lamprophyres have high Cr contents of 2260 – 2460 ppm, Ni of 720 – 770 ppm, and V of 120 – 134 ppm. The MgO, K_2O and Al_2O_3 plot shows their closeness to the kimberlite field (Fig. 6a), and their K_2O and SiO_2 ratios are akin to Shoshonite lamprophyres (Fig. 6b). Because the lamprophyres have undergone significant mineral alterations, the Nb/Y vs Zr/Ti and Sm vs Ce/Y ratios were used to classify them. These ratios show that the lamprophyres are subalkaline, particularly calc-alkaline in nature (Figs. 6c and 6d).

The granodiorites are characterized by moderate to high SiO_2 contents of 59.1 – 72.5 wt%, Na_2O of 2.5 – 4.2 wt%, and K_2O of 2 – 3.5 wt%, have low ferromagnesian oxides with Fe_2O_3t of 2.8 – 5.1 wt%, and MgO of 1.3 – 2.7 wt%, and high Al_2O_3 of 10.9 – 16.1 wt%. LOI contents of the granitoids are high in the range of 4.3 – 7.1 wt% and low Mg# of 47 – 51. These granitoids have been classified as calc-alkaline, I-type, and dominantly peraluminous on the AFM and A/CNK vs A/NK diagrams (Figs. 7a and 7b). On the total alkali vs Silica diagram, they plot as granodiorite, monzonite, and granite (Fig. 7c). However, they plot dominantly as granodiorite, with only one sample plotting as tonalite on the Ab-An-Or diagram (Fig. 7d). In terms of trace elements, the granodiorites have low Cr contents of 40 – 50 ppm, Ni of 10 – 30 ppm, and V of 22 – 42 ppm.

Fig. 8 shows chondrite normalised REE and primitive mantle-normalised multi-element plots for the lamprophyres and granitoids. Lamprophyres display enriched LREE and nearly flat HREE pattern (Fig. 8a). This REE pattern corresponds to high ratios of LREE to HREE (La/Yb of 6.6 – 8.4). The lamprophyres are also characterised by small negative Eu anomalies (Eu/Eu* = 0.78 – 0.91). Conversely, the granitoids exhibit LREE-enriched and HREE-depleted patterns (Fig. 8b), reflecting very high LREE/HREE (La/Yb = 17.2 – 21.9). They, however, show weak to pronounced positive Eu anomalies of Eu/Eu* = 1.02 – 1.43. On primitive mantle-normalised plots, the lamprophyres exhibit compatible element-depleted patterns characterised by high LILE and low HFSE, positive U and K, and negative Nb, Ta, Ti and Sr anomalies (Fig. 8c). Similarly, the granitoids display left-dipping patterns, characterised by high LILE and low HFSE, positive U, K, and Sr, and negative Nb, Ta, Sm, and Ti peaks (Fig. 8d).

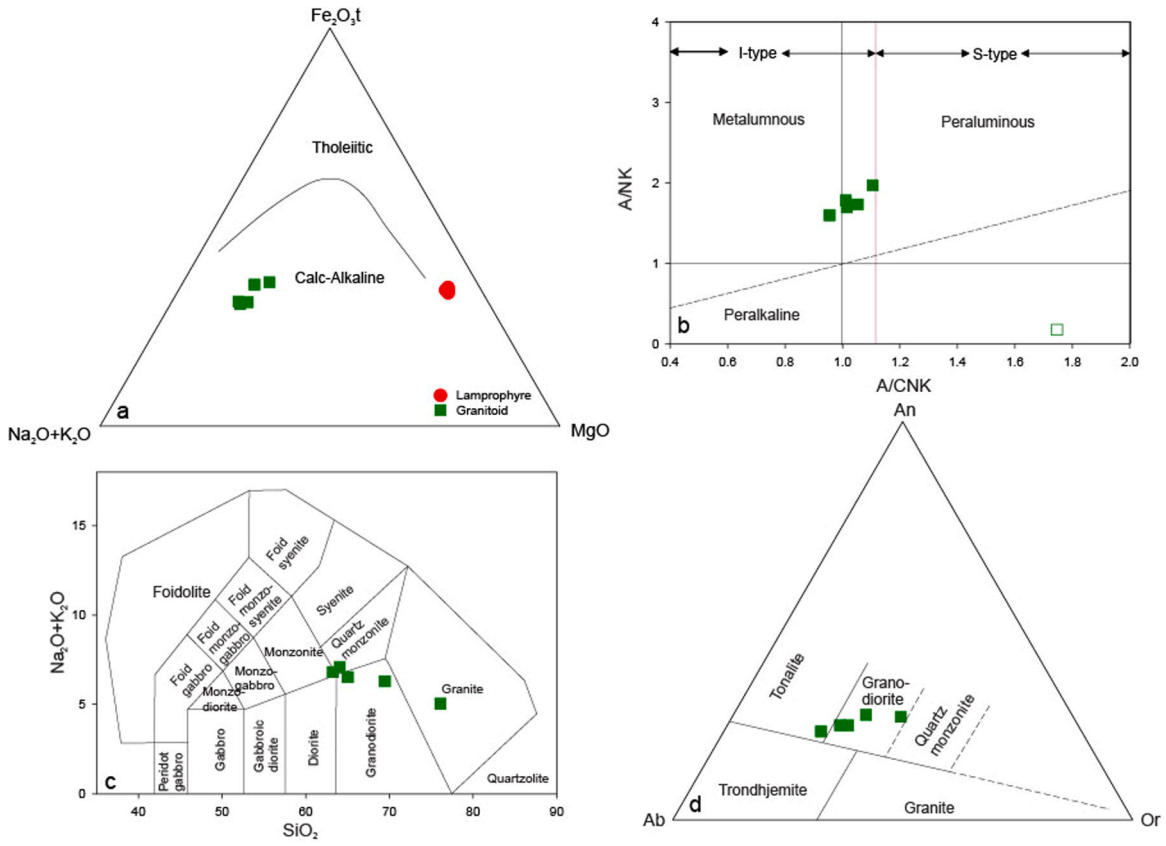

Fig. 7. Classification and magma characteristics of the Nampala Gold deposit granitoids and lamprophyre, (a) AFM diagram (after Irvine and Baragar, 1971), A/CNK vs A/NK diagram (after Maniar and Piccoli, 1989), (c) Total alkalis vs silica (TAS) (after Middlemost, 1994), and (d) Or-Ab-An ternary diagram (after O'Connor, 1965).

Zircon morphology, U-Pb ages and Lu-Hf isotope composition

Table 2 gives the zircon U-Pb ages for the studied sample. Sixty zircon grains were ablated for their U-Pb ages. Out of these, 25 were found to be concordant or nearly concordant zircons with age discordance < 7 % As a result, they were plotted using isoplot software and 21 of them were chosen for their Hf isotope study.

Fig. 9 illustrates the morphology and internal features of the zircon obtained from the granodiorite. The zircons are mostly euhedral to subhedral and generally have variable length and width ratios, with lengths from 150 μm to 280 μm and widths between 50 μm and 140 μm. Most zircon shows oscillatory and patchy zoning. The anhedral-granular grains are shown to be cloudy in nature on CL images, and their internal structures are clearly visible, displaying some inclusions and fissures.

No xenocrysts were observed, and the twenty least discordant grains yield an upper Concordia intercept age of 2100 ± 10 Ma and a weighted mean $^{207}Pb/^{206}Pb$ age of 2104 ± 8 Ma. This is considered to be Nampala's granitoid's crystallization period.

Table 3 provides the results of the analysis of twenty-one zircon grains for their Lu-Hf isotope signatures. The evaluated samples show similar depleted Lu-Hf isotope contents. Zircon grains from the granitoid, have $^{176}Hf/^{177}Hf$ readings of 0.281391 – 0.281536, corresponding to εHf(t) between −1.83 and 3.3(Fig. 11), and variable model ages: T^{1}_{DM} of 2.52 – 2.33 Ga and T^{2}_{DM} of 2.40 – 2.89 Ga (Table 3).

Discussion

Elemental mobility

Petrographic investigations have revealed that the Nampala Gold deposit lamprophyres have undergone significant mineral alterations, which may have affected the mobility of the major oxides and some trace elements. The post-magmatic alteration resulted in the high LOI (4.8 – 6.4 wt%) contents recorded for the lamprophyres. Nevertheless, because of auto-metasomatism, fresh lamprophyres can record high LOI contents (Jiang et al., 2010). To test if secondary alterations led to element mobility, bivariate plots of LOI and Zr vs major oxides and trace elements were plotted. Major oxides and trace elements show no obvious correlation with LOI, which may indicate insignificant mobility of these oxides and trace elements (Fig. 12). This deduction is supported by the plot of Zr vs major oxides and trace elements where there are coherent or linear trends (Fig. 13). Significant secondary alteration is also observed in the Nampala Gold deposit granitoids from the petrographic investigation, corresponding to high LOI contents (4.34 – 7.12 wt%). However, linear trends displayed on the plots of Zr vs major oxides and trace elements may argue for the insignificant mobility of these oxides and trace elements (Fig. 13).

Lamprophyre' petrogenesis

The effect of continental crustal contamination on lamprophyres will often result in an elevated SiO_2, which is not the case for the Nampala Gold deposit lamprophyres. Furthermore, continental crust, on average, has a Ba value of 325 ppm and Sr of 390 ppm (Rudnick and Fountain, 1995), whereas the lamprophyres from the Nampala Gold deposit have Ba of 210 – 270 ppm and Sr of 134 – 175 ppm. These values rule out significant continental crustal contamination. The Th/La and Lu/Yb concentrations are a good proxy to assess the effects of continental crustal contamination on lamprophyres. Typically, continental crust is characterised by high ratios of Th/La (>0.24) and Lu/Yb (0.16 – 0.18), whereas low ratios of Th/La (<0.24) and Lu/Yb (0.14 – 0.15) characterise mantle-derived magmas (Sun and McDonough, 1989; Rudnick and

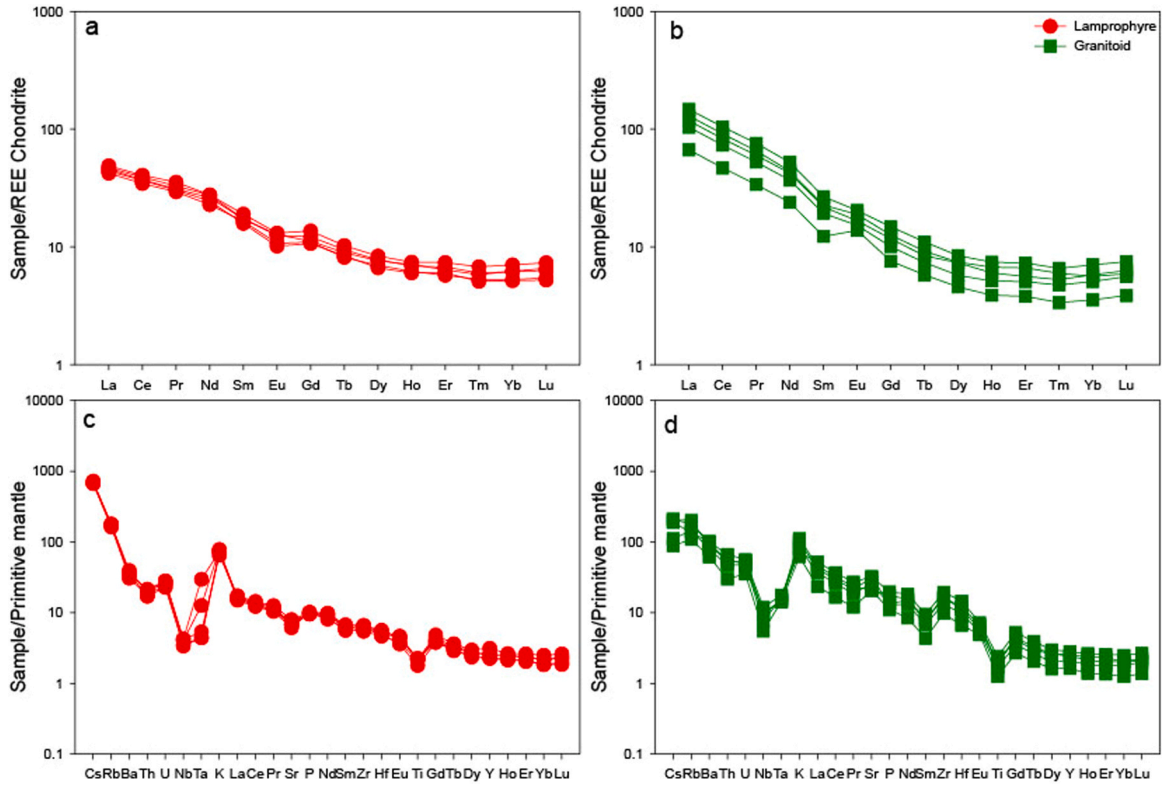

Fig. 8. Chondrite-normalised REE diagrams of (a) lamprophyres, and (b) granitoids of the Nampala Gold deposit: primitive mantle-normalised multi-elements diagrams of, (c) lamprophyres, and (d) granitoids of the Nampala Gold deposit. Chondrite and primitive mantle values are from Palme and O'Neil (2014).

Gao, 2003). The lamprophyres from the Nampala Gold deposit record Th/La ratios of 0.14 – 0.15 and Lu/Yb concentrations of 0.15 – 0.16, which are similar to mantle-derived magma, thus also ruling out significant continental crustal contamination. Therefore, there was no significant crustal contamination throughout the magmatic history of the Nampala Gold deposit lamprophyres.

The high Mg# of 77 – 78 indicates they were formed from near-primary magma (Li and Yan, 2021). Zr/Hf values of 39–41 are in agreement with the primitive mantle source (36.2 ± 2.0) (Taylor and McLennan, 1985; Stolz et al., 1996). Their relative enrichment of LREE to HREE may imply derivation from an enriched mantle source. However, this REE pattern could also suggest a low degree of partial melting or crustal contamination. The plots of Sr vs Cr and Ba vs V (Figs. 14a and 14b) show that the geochemical signatures of the Nampala Gold deposit lamprophyres result from fractional crystallization.

The high K_2O contents (Fig. 6c) coupled with the enriched-LILE concentrations (Fig. 8c) of the lamprophyres from the Nampala Gold deposit suggest the existence of amphibole and/or phlogopite in the mantle source, and this can be used to constrain the metosomatic history of the magma. Amphiboles and phlogopite are the main sources of LILE enrichments in the lithospheric mantle (Ionov et al., 1997; Wan et al., 2019). Mantle-source with phlogopite usually produces magma with high Ba/Rb (>0.1), and low Rb/Sr (<20) ratios (Furman and Graham, 1999). On the other hand, a high Rb/Sr ratio (>20) and low Ba/Rb ratio (<0.1) is characterised by mantle-source bearing amphibole (Furman and Graham, 1999). The Nampala Gold deposit lamprophyres recorded high Ba/Rb (0.56 – 0.79) and low Rb/Sr (2.04 – 2.50) ratio, plotting mainly in the phlogopite field (Fig. 14c); this suggests that they originated from a phlogopite-bearing mantle source.

To estimate the depth of melting of the Nampala Gold deposit lamprophyres, the ratios of Dy/Yb and Sm/Yb were used. Melting at deeper depth (i.e. garnet lherzolite stability field) produces high Dy/Yb (>2.4) and Sm/Yb (>2) ratios (Sun and McDonough, 1989; Wan et al., 2019). However, melting at shallow depth (i.e. spinel lherzolite stability field) yield low Dy/Yb (<1.5) and Sm/Yb (<1.4) values. The Dy/Yb and Sm/Yb values recorded for the Nampala Gold deposit lamprophyres are in the range between 1.8 and 2.0, and 2.5 and 2.9, respectively. These values imply that the magma for the Nampala Gold deposit lamprophyres was formed from the garnet-spinel transitional field. Experimental studies by McKenzie and O'Nions (1991), and Klemme and O'Neill (2000) revealed that the depth of the garnet-spinel lherzolite transitional field is between 75 and 85 km. Overall, the lamprophyres from the Nampala Gold deposit can be inferred as mantle-derived rocks, generated by a low degree of partial melting of phlogopite-bearing mantle sources in the transitional stability of the field of garnet-spinel at a depth between 75 and 85 km.

Tectonic setting of the lamprophyres

Mafic-ultramafic rocks with calc-alkaline geochemical signatures are mainly restricted to subduction zones, suggesting a subduction process in their formation (Winter, 2001). Hence, the calc-alkaline signatures exhibited by the Nampala Gold deposit lamprophyres suggest their emplacement in an arc environment. Magmas derived from MORB and OIB sources have an Nb/U ratio of 47 ± 7, whereas those from the crust have Nb/U ratios of 25 (lower crust) and 4.5 (upper crust) (Li and Yan, 2021). However, lower Nb/U ratios are observed when subduction-zone fluids play an important role in generating magma (Ayers, 1998; Foley et al., 2000). The Nb/U ratios obtained for the Nampala Gold deposit lamprophyres range from 3.51 – 4.04, plotting between primitive mantle and upper crust, which may indicate the influence of subduction component in their genesis (Fig. 15a). Furthermore, on a Ta/Yb vs Th/Yb diagram (Fig. 15b), the lamprophyres from the Nampala Gold deposit mostly plot in the active continental margin field, implying the influence of subduction-related processes or components in their evolution. Intraplate mafic rocks usually have low Ba/Nb and La/Nb ratios of 1 – 20 and 0.5 – 2.5 respectively (Jahn et al., 1999; Li and Yan, 2021). However, high values of Ba/Nb (>20) and La/Nb (>3) are characterised

Table 2
Zircon U-Pb ages data for the Nampala Gold deposit granodiorite.

Name	U	Th	Th/U	^{206}Pb	^{207}Pb/^{206}Pb*	1SE	^{208}Pb/^{206}Pb*	1SE	^{207}Pb/^{235}U*	Central (%)	207/206	1 s	207/235	1 s	206/238	1 s	208/232	1 s
NPT−11	205	25	0.12	86.9	0.13033	0.00106	0.03542	0.00601	7.20819	4.02	2102	14	2138	15	2174	27	2213	72
NPT−13	100	12.8	0.13	42.1	0.13314	0.00099	0.03634	0.00627	7.23823	0.16	2140	13	2141	13	2143	22	2128	67
NPT−17	230	23.9	0.10	92.3	0.13585	0.00102	0.0288	0.00583	7.15074	−4.86	2175	13	2130	18	2085	34	2019	68
NPT−18	193	13.1	0.07	82.7	0.13211	0.00114	0.02144	0.00371	7.25962	1.99	2126	14	2144	15	2162	26	2370	92
NPT−29	107	16.5	0.15	46.4	0.13568	0.00125	0.04454	0.00801	7.45946	−0.52	2173	16	2168	16	2163	29	2183	86
NPT−32	227	21.6	0.10	93.2	0.12932	0.00118	0.02672	0.00455	6.81443	−0.13	2089	15	2088	14	2086	24	2049	72
NPT−39	135	12.3	0.09	72.9	0.15955	0.00283	0.05017	0.00971	10.22884	0.52	2451	29	2456	24	2461	39	4588	323
NPT−43	292	20.2	0.07	118	0.13309	0.00156	0.02841	0.00554	6.89453	−4.53	2139	19	2098	56	2056	110	2874	116
NPT−44	79	10.7	0.14	34.5	0.14318	0.00154	0.04473	0.00797	7.91912	−4.77	2266	18	2222	24	2174	44	2494	96
NPT−48	207	17	0.08	96.7	0.15749	0.00288	0.04348	0.00885	9.30646	−6.33	2429	30	2369	28	2299	46	4102	225
NPT−50	243	22.9	0.09	96.9	0.12922	0.00137	0.02829	0.00508	6.53505	−4.07	2087	19	2051	24	2014	44	2102	92
NPT−56	285	44.8	0.16	119.5	0.12968	0.00144	0.04319	0.00753	6.86706	0.09	2094	19	2094	19	2095	33	2010	87
NPT−60	288	25	0.09	124.3	0.13017	0.00151	0.02425	0.00427	7.03579	1.78	2100	19	2116	21	2132	38	2088	98
NPT−65	194	8.4	0.04	90.1	0.14491	0.00194	0.0116	0.00224	8.13742	−4.34	2287	22	2246	22	2202	37	2081	124
NPT−72	266	26.3	0.10	110.5	0.12987	0.00177	0.02639	0.00473	6.61229	−3.91	2096	24	2061	21	2026	34	1885	107
NPT−74	180	15.9	0.09	79.1	0.12864	0.00182	0.02405	0.00435	6.91513	2.41	2080	25	2101	22	2122	37	2016	126
NPT−75	94	8.7	0.09	41.1	0.13153	0.00193	0.02439	0.00435	7.02573	−0.42	2118	25	2115	23	2111	39	1960	111
NPT−83	592	39.3	0.07	264	0.13015	0.00195	0.01939	0.00359	7.07223	2.34	2100	25	2121	24	2142	41	2186	137
NPT−87	183	14.3	0.08	74.8	0.12905	0.0019	0.02025	0.00373	6.41206	−5.64	2085	26	2034	23	1984	36	1790	108
NTP−91	99	19.2	0.19	44.8	0.13792	0.00239	0.0548	0.01069	7.43368	−3.96	2201	28	2165	26	2127	43	2102	150
NPT−99	137	9.5	0.07	60.3	0.12939	0.00214	0.0182	0.00343	6.87933	0.72	2090	28	2096	26	2102	43	1932	139
NPT−101	246	19.5	0.08	109.4	0.12957	0.00278	0.02251	0.00431	6.96511	1.69	2092	37	2107	32	2122	53	2107	152
NPT−105	257	33.8	0.13	109	0.13013	0.0018	0.03616	0.00682	6.59252	−4.57	2100	24	2058	26	2017	46	1932	129
NPT−108	171	14.5	0.08	77.4	0.13736	0.00193	0.02341	0.00433	7.41315	−3.46	2194	24	2163	27	2129	49	2061	140
NPT−110	135	9.1	0.07	73.8	0.16947	0.00302	0.04293	0.00928	11.24585	−0.92	2552	29	2544	40	2533	83	5366	421

by arc-related mafic rocks (Jahn et al., 1999). On the plot of La/Nb vs Ba/Nb (Fig. 15c), the Nampala Gold deposit lamprophyres show elemental ratios similar to arc-related rocks. The negative peaks of Nb, Ta, and Ti displayed by the lamprophyres on the primitive mantle-normalised multi-element diagram (Fig. 8c) points to subduction-zone processes in their genesis (Elburg, 2010). Thus, the lamprophyres from the Nampala Gold deposit were most likely formed in an arc setting during the subduction process of the Eburnean orogeny.

Petrogenesis of the granodiorites

The geochemical data in Table 1 indicates that the granodiorites from the Nampala Gold deposit have low Mg# (Mg# = 47–51) and low Ni (10 – 30 ppm), Co (23 – 45 ppm) and Cr (30 – 50 ppm) contents. These geochemical characteristics suggest that these rocks were formed from evolved magma rather than primary magma (Wilson, 1989; Winter, 2001). These granodiorites have I-type peraluminous features, exhibiting a high-K calc-alkaline nature (Figs. 7a and 7d). This calc-alkaline characteristic and its I-type nature may indicate the melting of older igneous crustal materials (Gläser et al., 2022). On a chondrite-normalised REE diagram (Fig. 8b), the granodiorites show enrichment in LREE compared to HREE, showing a weak to pronounced positive Eu anomaly (Eu/Eu* = 1.04 – 1.14). These REE patterns, along with positive peaks in Ba, Sr, and Eu, could be linked to the presence of plagioclase at the source or the formation of magmas in a reduced environment, such as the lower continental crust or upper mantle (Rudnick and Gao, 2014).

The Nampala Gold deposit granodiorites display a depletion in Ti, Nb, and Ta on the primitive-mantle normalized multi-element plot (Fig. 8d), alongside weak positive Zr-Hf anomalies. These geochemical signatures are indicative of continental crust origin (Elburg, 2010; Rudnick and Gao, 2014). Additionally, the granitoids exhibit low Sr/Y ratios, with high Yb (>1.0 ppm) and Y (>10 ppm) contents, further suggesting that their formation involved the melting of crustal material. On the SiO_2 versus Mg# diagram (Fig. 16), the granodiorites of the Nampala Gold deposit plot in the delaminated lower crust-derived granodiorites region. Their Nb content and Nb/U ratios are similar to lower crust (Fig. 15a). This indicates the melting of the delaminated lower crust to form the Nampala Gold deposit granodiorites.

Tectonic setting

To evaluate the tectonic context of the Nampala Gold deposit granodiorites, a number of tectonic discrimination diagrams have been employed together with trace element patterns and ratios. The Nampala Gold deposit granodiorites have depleted HFS and enrichment of LILE in their overall trace element patterns, while Nb-Ta and Ti exhibit negative peaks (Figs. 8b and 8d). Generally, these geochemical characteristics have been interpreted as signatures of subduction processes (Elburg, 2010; Spandler and Pirard, 2013; Kelemen et al., 2014). (Fig. 17a) also supports their formation in an arc environment. Fig. 17b according to; (Thiéblemont & Tégyey, 1994) defines the Nampala Gold deposit granodiorites as either island arcs-related or continental margins-related. However, their Nb/Yb and Th/Yb ratios discriminate them as continental arc granitoids (Fig. 17c). The Nampala Gold deposit granodiorites are classified into different orogenic phases according to the R1 (4Si-11(Na+K)-2(Fe+Ti)) vs R2 (6Ca+2Mg+Al) diagram (Fig. 17d; Batchelor and Bowden, 1985). The granodiorites plot as mantle fractionates and pre- to syn-collision, suggesting that they may have formed during the subduction-accretion phase of the Eburnean orogeny.

Timing of emplacement of the granodiorites

Southern Mali has received some degree of attention in terms of geochronological studies.

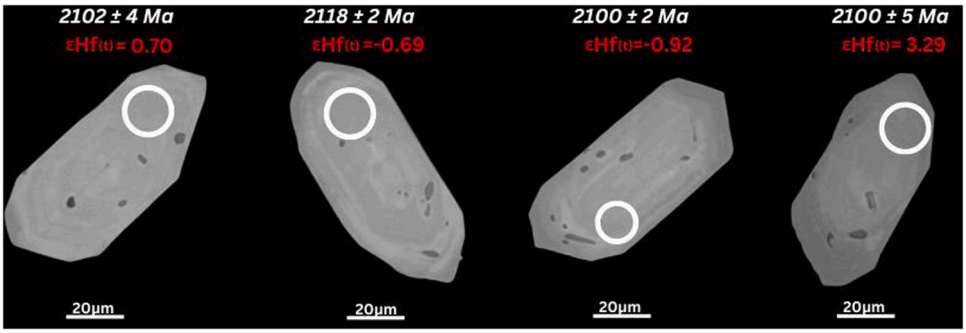

Fig. 9. Representative cathodoluminescence images CL images for representative zircons analysed for U-Pb and Lu-Hf measurement, the white circles indicate spot location.

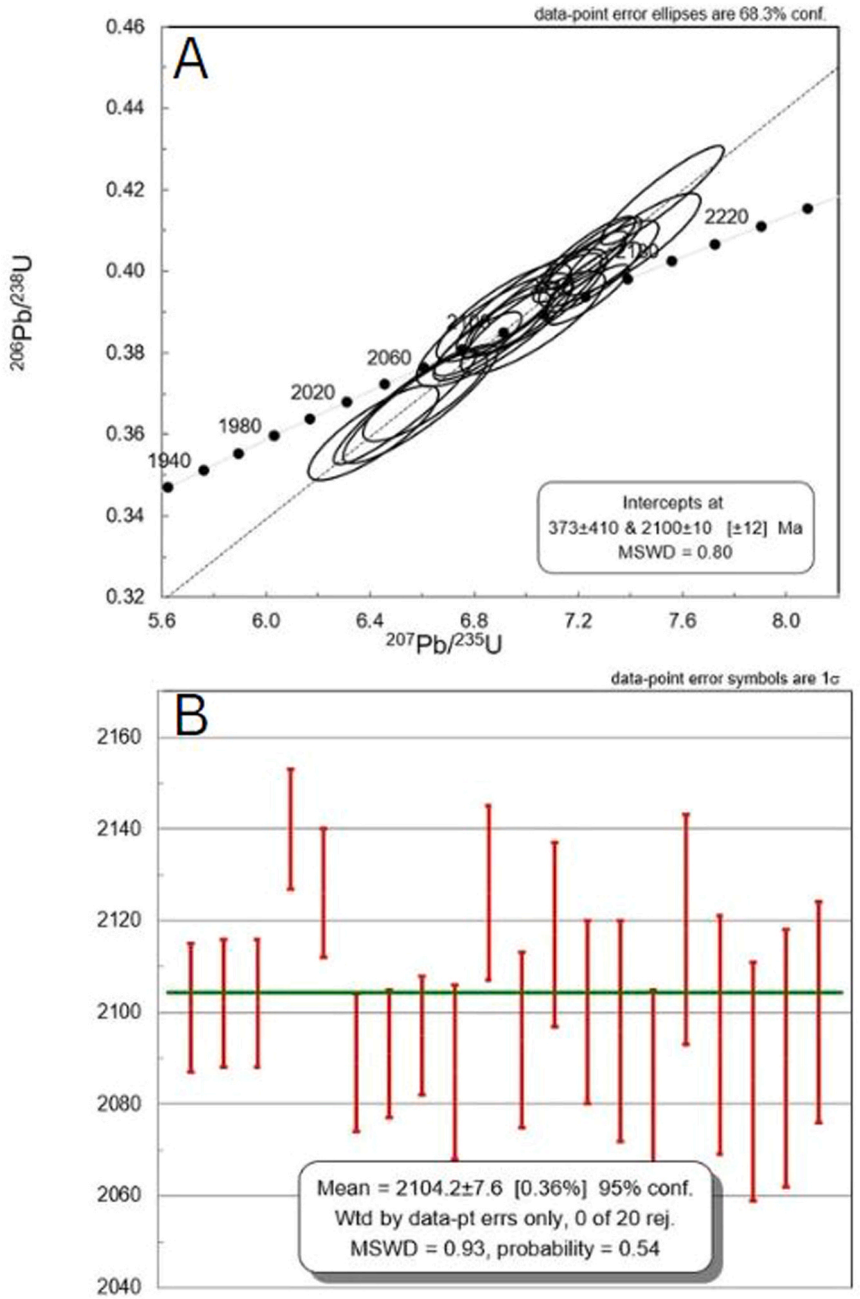

Fig. 10. A- Zircon U-Pb concordia diagram 2100 ± 10 Ma and B- weighted mean $^{207}Pb/^{206}Pb$ age 2104 ± 8 Ma.

Table 3
Zircon Lu-Hf isotope data for the Nampala Gold deposit granodiorite.

Spot	$^{176}Yb/^{177}Hf$	±(1σ)	$^{176}Lu/^{177}Hf$	±(1σ)	$^{176}Hf/^{177}Hf$	±(1σ)	t* (Ma)	$(^{176}Hf/^{177}Hf)_i$	$\varepsilon_{Hf}(t)$	±(1σ)	Age (Ma)	TDM (Ga)	TDM2 (Ga)
NPT−13	0.0549	0.000113	0.001988	7.99E−06	0.281524	1.56E−05	2100	0.281444	0.04	0.546	2140000000	2.45	2.80
NPT−18	0.041183	0.000186	0.001333	9.5E−06	0.281533	7.77E−06	2100	0.281479	1.30	0.27195	2126000000	2.40	2.67
NPT−29	0.01883	0.000105	0.000594	3.03E−06	0.281484	6.75E−06	2100	0.28146	0.61	0.23625	2173000000	2.42	2.62
NPT−32	0.059856	0.000696	0.00211	3.21E−05	0.281515	1.35E−05	2100	0.281431	−0.43	0.4725	2089000000	2.47	2.86
NPT−39	0.032876	0.000208	0.00103	6.74E−06	0.281546	7.95E−06	2100	0.281504	2.19	0.27825	2451000000	2.36	2.40
NPT56	0.059684	0.000506	0.001965	7.93E−06	0.281536	1.36E−05	2100	0.281458	0.52	0.476	2094000000	2.44	2.79
NPT60	0.052595	0.000407	0.001935	2.21E−05	0.281527	1.45E−05	2100	0.28145	0.25	0.5075	2100000000	2.45	2.80
NPT−65	0.0242	9.22E−05	0.000906	5.06E−06	0.281428	8.7E−06	2100	0.281391	−1.83	0.3045	2287000000	2.52	2.73
NPT−74	0.054863	0.000878	0.002099	3.23E−05	0.281516	1.93E−05	2100	0.281432	−0.39	0.6755	2080000000	2.47	2.86
NPT−75	0.043734	0.000744	0.00166	2.97E−05	0.28149	1.73E−05	2100	0.281424	−0.69	0.6055	2118000000	2.48	2.82
NPT−83	0.050653	0.000498	0.001939	1.25E−05	0.281495	1.62E−05	2100	0.281417	−0.92	0.567	2100000000	2.49	2.87
NPT−91	0.021524	0.000126	0.000679	4.78E−06	0.281501	6.95E−06	2100	0.281474	1.09	0.24325	2201000000	2.40	2.58
NPT−99	0.050737	0.000377	0.001792	2.02E−05	0.281519	8.81E−06	2100	0.281447	0.15	0.30835	2090000000	2.45	2.80
NPT−101	0.067462	0.000795	0.002446	2.68E−05	0.281565	2.29E−05	2100	0.281467	0.85	0.8015	2092000000	2.43	2.81
NPT−105	0.057302	0.000366	0.001738	9.53E−06	0.281605	9.03E−06	2100	0.281536	3.29	0.31605	2100000000	2.33	2.60
NPT−108	0.053283	0.000744	0.00216	3.35E−05	0.281501	1.42E−05	2100	0.281415	−1.01	0.497	2194000000	2.50	2.85
NPT−110	0.075715	0.000782	0.002502	1.64E−05	0.281543	0.00002	2100	0.281443	0.01	0.7	2552000000	2.46	2.63
NPT−50	0.059728	0.00078	0.002117	3.05E−05	0.281539	1.45E−05	2100	0.281454	0.39	0.5075	2087000000	2.44	2.81
NPT−44	0.039071	0.000136	0.001311	1.08E−05	0.281507	1.09E−05	2100	0.281455	0.42	0.3815	2266000000	2.43	2.64
NPT−11	0.036433	0.000266	0.001171	5.66E−06	0.281509	7.58E−06	2100	0.281463	0.70	0.2653	2102000000	2.42	2.71
NPT−43	0.078219	0.00122	0.002841	4.56E−05	0.281547	1.57E−05	2100	0.281434	−0.33	0.5495	2139000000	2.48	2.89

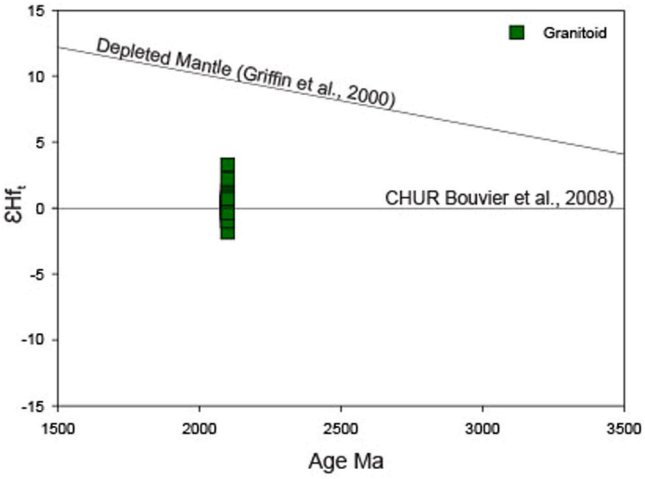

Fig. 11. Age vs εHft for the granitoid of the Nampala Gold deposit.

Table 4
Modal Composition of granodiorite.

Minerals	NFD1	NFD2	NFD3	NFD4
Quartz	25	27	28	26
Plagioclase	23	22	23	25
Dolomite	17	15	12	12
mica	23	20	22	15
Clinochlore	-	-	-	10
Opaque mineral	5	6	5	4
K-feldspar	-	5	-	-
Microcline	4	5	4	3
Kaolinite	3	-	6	-
Diopside	-	-	-	5
Total	**100**	**100**	**100**	**100**

Table 5
Modal Composition of Lamprophyre.

Minerals	NFC1	NFC2	NFC3	NFC4
Quartz	7	8	7	6
Calcite	7	6	12	8
Amphibole	13	13	12	13
mica	19	18	17	20
Clinochlore	23	22	21	22
Opaque mineral	5	6	5	4
Talc	26	27	26	27
Total	**100**	**100**	**100**	**100**

The Massigui region and the Bagoe basin are separated by the Banifing shear zone and are comprised of Paleoproterozoic plutonic rocks intruding into the meta volcano-sedimentary series. In the Massigui region granitoids and dioritoids' zircon SHRIMP U-Pb ages point to a significant magmatic phase around 2100 Ma (Wane et al., 2018). The Massigui quartz monzodiorite has an age of 2112 ± 5 million years, the granodiorite has an age of 2103 ± 5 million years, the pink quartz monzonite has an age of 2095 ± 9 million years, the Syobougou quartz microdiorite has an age of 2102 ± 10 million years, and the Tiéfala foliated quartz micromonzodiorite has an age of 2106 ± 11 million years (Wane et al., 2018).

The concordia age of 2100 ± 10 Ma for the granodiorite (Fig. 10) agrees with (Wane et al., 2018) As a result, the Banifing shear zone magmatic episode possibly continued for 20–30 Ma (Liegois et al., 1991). The geochronology of the plutons and the structural evidence demonstrate a close relationship between the plutons and the transpressive kinematics, suggesting that the Banifing Shear Zone was tectonically productive from 2115 to 2095 Ma, as shown by the greatest

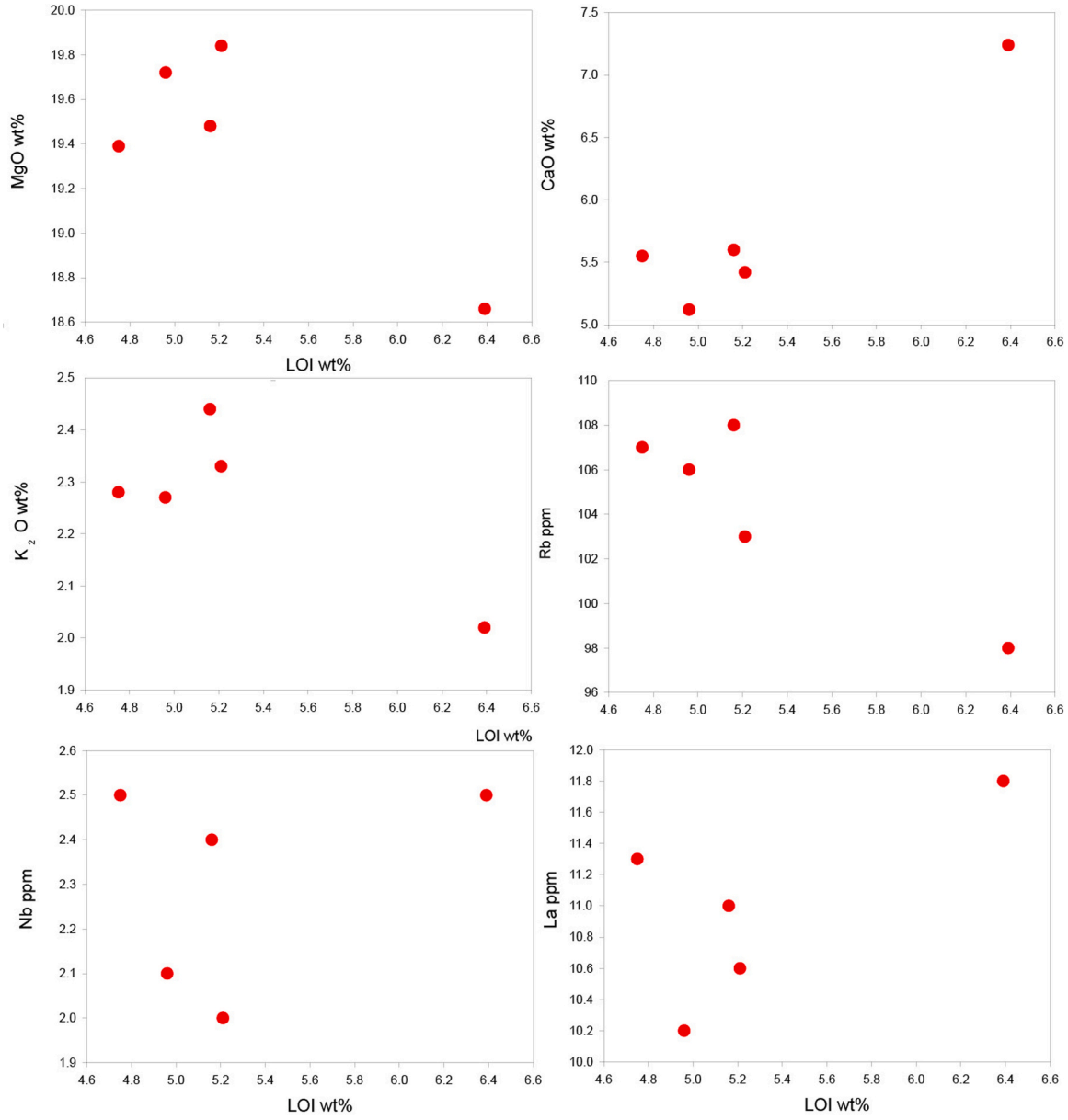

Fig. 12. Bivariate plot of LOI vs selected major oxides and trace elements.to evaluate the elemental mobility of the Nampala Gold deposit lamprophyres.

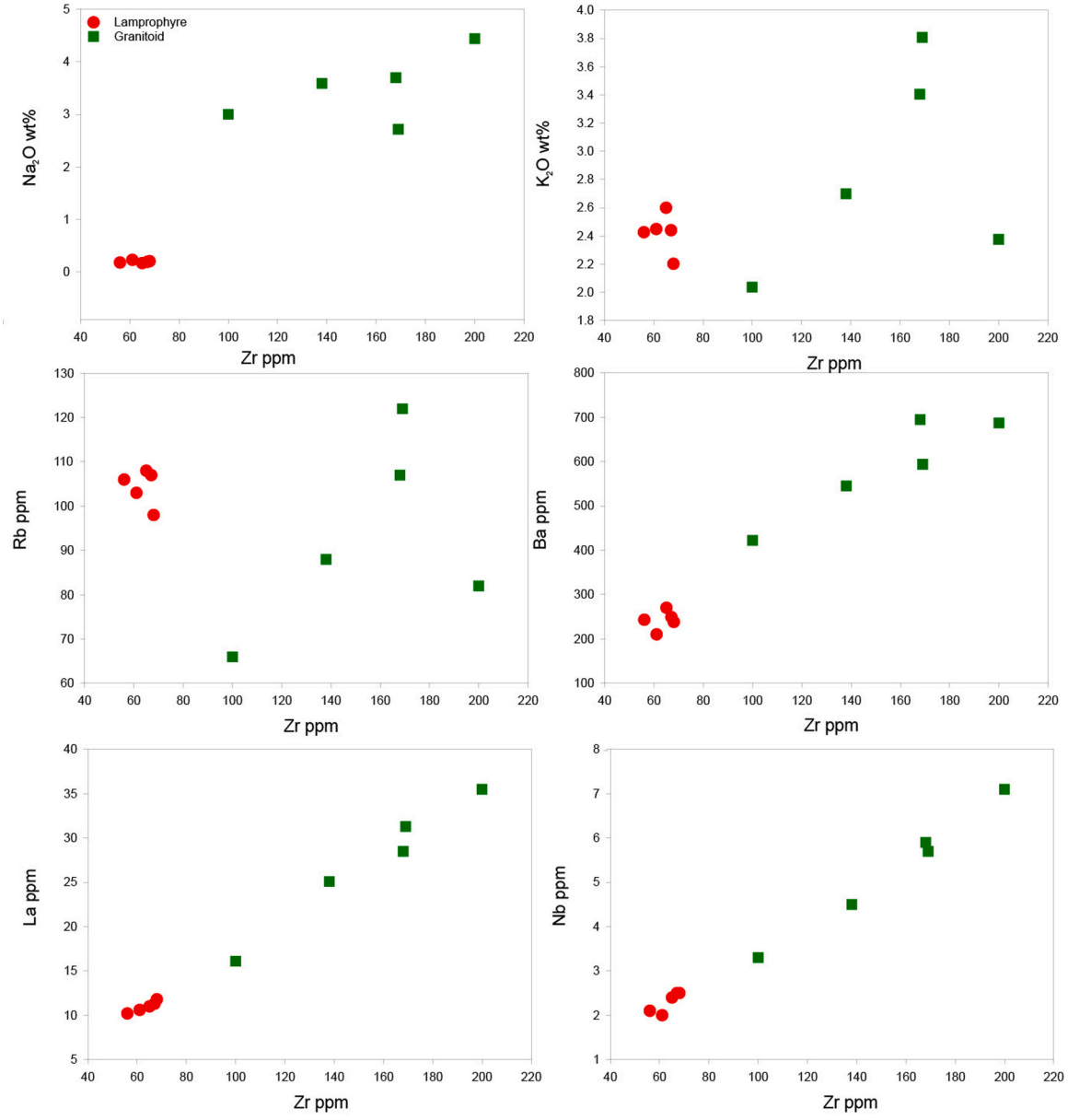

Fig. 13. Bivariate plot of Zr vs selected major oxides and trace elements to evaluate the elemental mobility of the Nampala Gold deposit lamprophyres and granitoids.

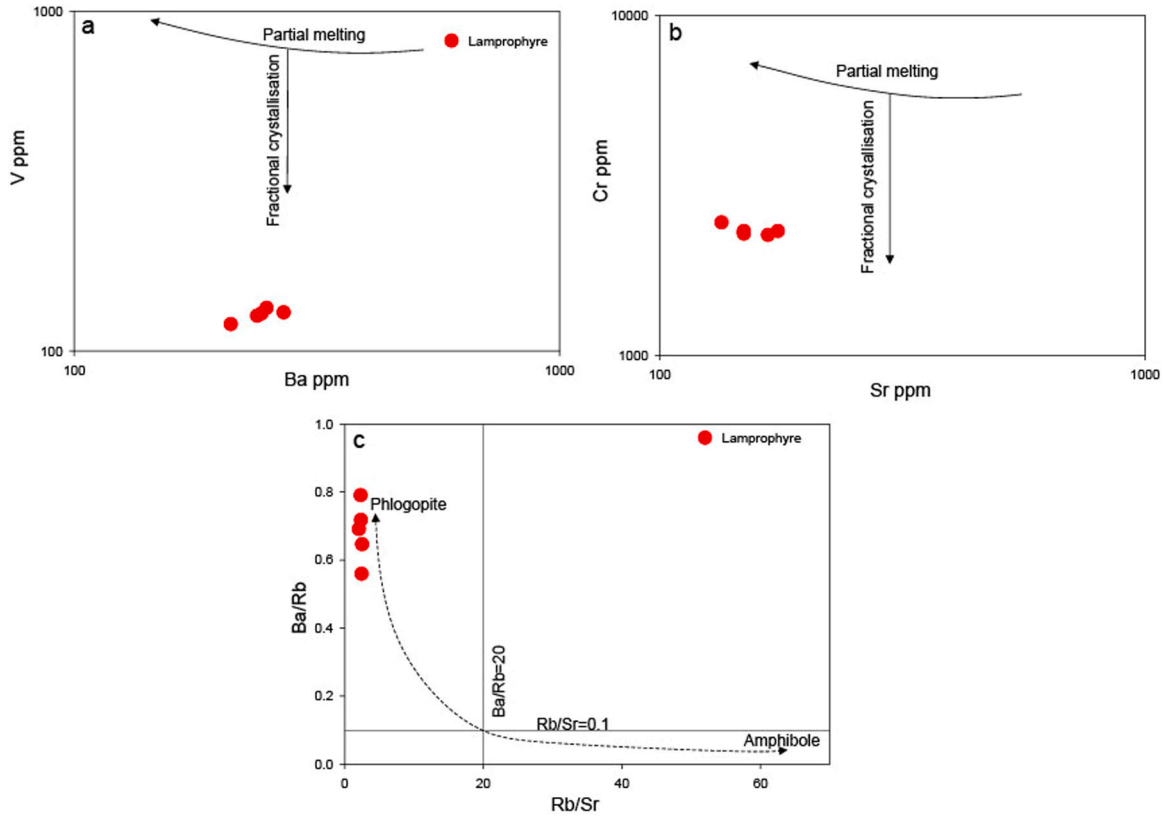

Fig. 14. Plots of incompatible elements vs compatible elements (a) Ba vs V, and (b) Sr vs Cr) showing the influence of partial melting on the distribution of elements for the Nampala Gold deposit lamprophyres, (c) Ba/Rb vs Rb/Sr diagram (after Furman and Graham, 1999), which shows that the Nampala Gold deposit lamprophyres were sourced from phlogopite-bearing mantle.

increase in magmatic intensity. Nevertheless, the shear zone probably remained to serve as the primary crustal funnel that channelled subsequent smaller magmatic episodes.

It has been suggested that an early Paleoproterozoic crust, which formed between 2.20 and 2.14 Ga, was reworked during the 2.14 Ga to 2.10 Ga Eburnean orogeny through magmatism, metamorphism, and deformation (Sakyi et al., 2014; Anum et al., 2015; Amponsah et al., 2023). High $\varepsilon Hf_{(t)}$ values of $> >0$ correspond to juvenile mantle input, whereas low $\varepsilon Hf_{(t)}$ $< <0$ suggest remelting of older continental crust, with values close to zero potentially implying mixing of older crust and depleted mantle (Kröner et al., 2013). Accretionary orogens are broad, consist of juvenile crust, and have mantle melts with limited crustal staying times(Chardon et al., 2009, Traoré et al., 2022). Thus, the subchondritic $\varepsilon_{Hf}(t)$ values between −1.83–3.3 (Fig. 11), and variable model ages, TDM1 of 2.52 – 2.33 Ga, for the granitoid may indicate a mixture of juvenile mantle melts and recycled older Paleoproterozoic crust during an accretionary orogen. This implies the occurrence of complex geological events and long periods of magmatic activity.

Geodynamic significance to the evolution of the WAC

The Rhyacian Eburnean orogeny led to the occurrence of the Birimian Paleoproterozoic rocks (Abouchami et al., 1990; Baratoux et al., 2011; Sakyi et al., 2019). Several years of geochemical studies have revealed that subduction-accretion mechanisms had a role in their formation and evolution (Dampare et al., 2008; Senyah et al., 2016; Sakyi et al., 2018; 2020; McFarlane et al., 2019). The Birimian granitoids and mafic rocks exhibit trace element signatures that are typical of arc crust, including variable enrichment of LILE, depletion of HFSE, positive Pb anomalies, and consistent negative Nb-Ta troughs, Ti peaks (Dampare et al., 2008; Senyah et al., 2016; Sakyi et al., 2018; 2020). These geochemical features are observed in the Nampala Gold deposit lamprophyres and granitoids. These rocks, specifically the granitoids formed during the 2.1 Ga tectonomagmatic Eburnean events, represent a mix of juvenile arc crust and recycled older Paleoproterozoic crust formed in subduction zone. Thus, our results provide significant insights into the subduction-accretion processes involved in the development of the Birimian Terrane within the West African Craton.

Conclusion

- The lamprophyres are sub-alkaline, particularly calc-alkaline in nature.
- The lamprophyres from the Nampala Gold deposit can be inferred as mantle-derived rocks originating from a low degree of partial melting.
- The geochemical signature of the lamprophyres suggests they formed from phlogopite-bearing lherzolite in the spinel-garnet transition field at depths between 75 and 80 km.
- The granitoids are classified as granodiorite with I-type, peraluminous and high-K calc-alkaline signatures, having 2.1 Ga as crystallization age.
- The subchondritic $\varepsilon_{Hf}(t)$ values of −1.83–3.3, coupled with the variable model ages, T^1_{DM} of 2.52 – 2.33 Ga, for the granodiorites may indicate a mixture of juvenile mantle melts and recycled older Paleoproterozoic crust during an accretionary orogen.
- The Mg# and SiO_2 contents, together with REE patterns and positive peaks in Ba, Sr, and Eu, could suggest the melting of the delaminated lower crust to form the granitoids.
- Geochemical data indicate a subduction process was significant in the formation of the lamprophyres and granitoids of the Nampala Gold deposit.

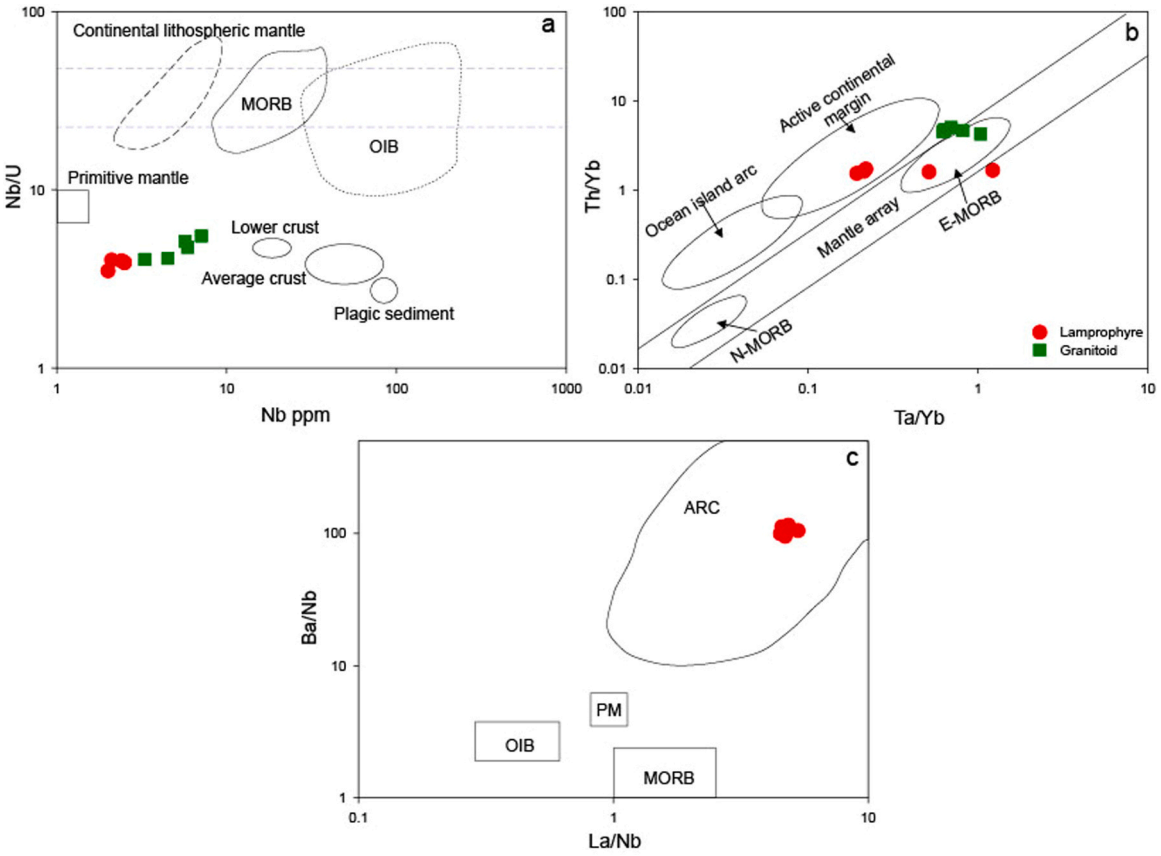

Fig. 15. Tectonic discrimination plots for the Nampala Gold deposit lamprophyres (a) Nb vs Nb/U, (b) Ta/Yb vs Th/Yb, and (c) La/Nb vs Ba/Nb.

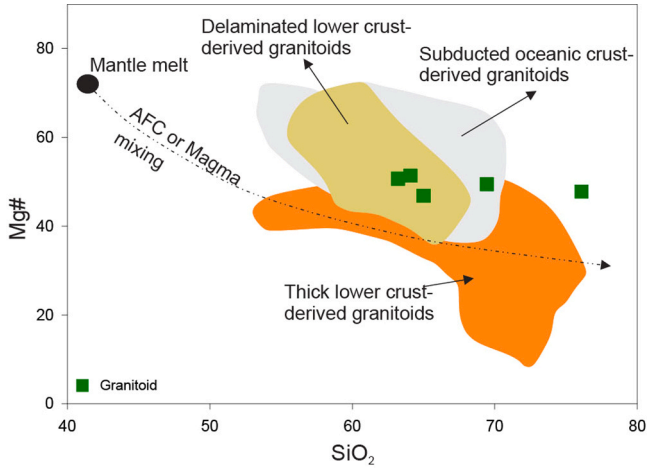

Fig. 16. SiO_2 vs. Mg# plot for the Nampala Gold deposit granitoids for petrogenetic interpretation. The fields regarding mantle, subducted oceanic crust, pure oceanic crust, delaminated lower crust, and thick lower crust, are from Wang et al. (2007).

- Thus, our results provide important constraints on the subduction-accretion process postulated to explain the evolution of the West African Craton's Birimain Terrain.

Funding

The research has been financed by the African Union (AU) Commission.

CRediT authorship contribution statement

Kazapoe Raymond Webrah: Writing – review & editing. **Kwayisi Daniel:** Writing – review & editing, Visualization, Data curation, Conceptualization. **Bolarinwa Anthony T.:** Writing – review & editing, Supervision. **Bouare Mamadou L.:** Writing – review & editing, Supervision. **KONATE Sory I.M.:** Writing – original draft, Methodology, Data curation, Conceptualization. **N'Dah N.'Tcha Daniel Kouagou:** Writing – review & editing. **Traore Elhadji Mory:** Writing – review & editing.

Declaration of Competing Interest

The authors declare that they have no known competing financial interests or personal relationships that could have appeared to influence

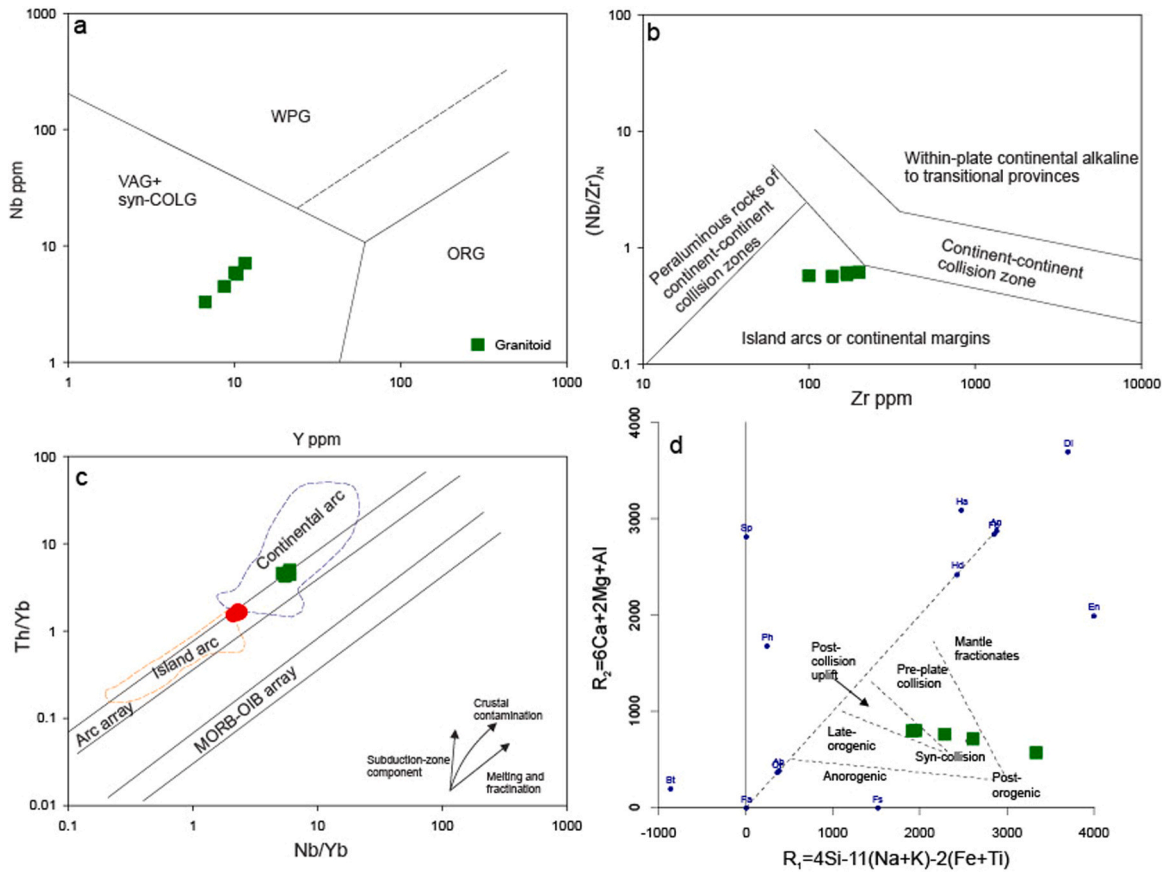

Fig. 17. Tectonic discriminant diagrams for the Nampala Gold deposit lamprophyres and granitoids (a) Nb vs. Y (after Pearce et al., 1984), (b) Zr vs. (Nb/Zr)N diagram (after Thiéblemont and Tégyey, 1994), (c) Th/Yb vs. Nb/Yb with reference fields modified after Pearce et al. (2008), and (d) R1-R2 (after Batchelor and Bowden, 1985).

the work reported in this research paper.

Acknowledgement

The present research shows a partial outcome of the first author's ongoing PhD project at the Pan African University Life and Earth Sciences Institute (including Health and Agriculture) (PAULESI), University of Ibadan, Ibadan, Nigeria. The first author is grateful to the African Union for its financial support, as well as to Adama Arama, the chief Exploration geologist at Nampala, and the whole exploration team. Special thanks to Prof. Andrew Kerr for his editorial contributions to the manuscript.

Appendix A. Supporting information

Supplementary data associated with this article can be found in the online version at doi:10.1016/j.rines.2025.100070.

Data availability

Data will be made available on request.

References

Abouchami, W., Boher, M., Michard, A., Albarede, F., 1990. A major 2.1 Ga event of mafic magmatism in West Africa: an early stage of crustal accretion. J. Geophys. Res.: Solid Earth 95 (B11), 17605–17629.

Agangi, A., Hofmann, A., Elburg, M.A., 2018. A review of Palaeoarchaean felsic volcanism in the eastern Kaapvaal craton: Linking plutonic and volcanic records. Geoscience Frontiers 9 (3), 667–688.

Agra, N.A., Elburg, M.A., Vorster, C., 2023. Constraints on Paleoproterozoic crustal growth from Birimian Supergroup lavas of the Bui belt (Ghana) in the West African Craton. Precambrian Research 384, 106926.

Amponsah, P.O., Kwayisi, D., Awunyo, E.K., Sapah, M.S., Sakyi, P.A., Su, B.X., Lu, Y., Nude, P.M., 2023. New evidence for crustal reworking and juvenile arc-magmatism during the Palaeoproterozoic Eburnean events in the Suhum Basin, South-east Ghana. Geol. J. 58 (10), 3734–3755.

Andersen, T., Elburg, M.A., van Niekerk, H.S., Ueckermann, H., 2018. Successive sedimentary recycling regimes in southwestern Gondwana: Evidence from detrital zircons in Neoproterozoic to Cambrian sedimentary rocks in southern Africa. Earth-Science Reviews 181, 43–60.

Anum, S., Sakyi, P.A., Su, B.-X., Nude, P.M., Nyame, F., Asiedu, D., Kwayisi, D., 2015. Geochemistry and geochronology of granitoids in the Kibi-Asamankese area of the Kibi-Winneba volcanic belt, southern Ghana. J. Afr. Earth Sci. 102, 166–179.

Ayers, J., 1998. Trace element modelling of aqueous fluid peridotite interaction in the mantle wedge of subduction zones. Contrib. Mineral. Petrol. 132, 390–404.

Ballo, I., Hein, K.A., Guindo, B., Sanogo, L., Ouologuem, Y., Daou, G., Traore, A., 2016. The Syama and Tabakoroni goldfields, Mali. Ore Geol. Rev. 78, 578–585.

Baratoux, L., Metelka, V., Naba, S., Jessell, M.W., Grégoire, M., Ganne, J., 2011. Juvenile Paleoproterozoic crust evolution during the Eburnean orogeny (~ 2.2–2.0 Ga), western Burkina Faso. Precambrian Res. 191 (1-2), 18–45.

Batchelor, B., Bowden, P., 1985. Petrogenetic interpretation of granitoid rock series using multinational parameters. Chem. Geol. 48, 43–55.

Bentley, P.N., Venter, L., Moolman, R., Henry, G., Heidstra, P., Reading, D., 2000. Geological review, gold target prioritisation and recommendations for future exploration work. Syama Exploration Permits Randgold Resources Ltd. internal report, unpublished.

Bergman, S.C. (1987). Lamproites and other potassium-rich igneous rocks: a review of their occurrence, mineralogy and geochemistry. *Geological Society, London, Special Publications*, *30*(1), 103-190.

Chardon, D., Gapais, D., Cagnard, F., 2009. Flow of ultra-hot orogens: a view from the Precambrian, clues for the Phanerozoic. Tectonophysics 477 (3–4), 105–118. https://doi.org/10.1016/j.tecto.2009.03.008.

Dampare, S., Shibata, T., Asiedu, D., Osae, S., Banoeng-Yakubo, B., 2008. Geochemistry of Paleoproterozoic metavolcanic rocks from the southern Ashanti volcanic belt, Ghana: petrogenetic and tectonic setting implications. Precambrian Res. 162 (3-4), 403–423.

Elburg, M.A., 2010. Sources and processes in arc magmatism: The crucial role of water (An inaugural lecture to the Society). Geol. Belg.

Foley, S.F., Barth, M.G., Jenner, G.A., 2000. Rutile/melt partition coefficients for trace elements and an assessment of the influence of rutile on the trace element characteristics of subduction zone magmas. Geochim. Cosmochim. Acta 64, 933–938.

Furman, T., Graham, D., 1999. Erosion of lithospheric mantle beneath the East African Rift system: geochemical evidence from the Kivu volcanic province. Dev. Geotecton. 24, 237–262.

Girard, P., Goulet, N. & Malo, M., 1998. La géologie du Mali. Projet Assistance Technique au Secteur Minier du Mali. Crédit IDA 2390-MLI. Rapp. DNGM, Bamako, Mali, n°5951, 108p.

Gläser, L., Grosche, A., Voudouris, P.C., Haase, K.M., 2022. The high-K calc-alkaline to shoshonitic volcanism of Limnos, Greece: implications for the geodynamic evolution of the northern Aegean. Contrib. Mineral. Petrol. 177 (8), 73.

Irvine, T.N., Baragar, W.R.A., 1971. A guide to the chemical classification of the common volcanic rocks. Canadian Journal of Earth Sciences v. 8, 523–548.

Jahn, B.M., Wu, F.Y., Lo, C.H., 1999. Crust–mantle interaction induced by deep subduction of the continental crust: geochemical and Sr–Nd isotopic evidence from post-collisional mafic–ultramafic intrusions of the northern Dabie Complex, Central China. Chem. Geol. 157, 119–146.

Jiang, Y.H., Jiang, S.Y., Ling, H.F., Ni, P., 2010. Petrogenesis and tectonic implications of Late Jurassic shoshonitic lamprophyre dikes from the Liaodong Peninsula, NE China. Min. Petrol. 100, 127–151.

Kelemen, P.B., Hanghoj, K., Greene, A.R., 2014. One view of the geochemistry of subduction-related magmatic arcs, with an emphasis on primitive andesite and lower crust. *Treatise Geochem.* 4, 749–805.

Kerr-Gillespie, F., Kinnan, E., Carrier, A., 2018. NI 43-101 technical report for the nampala and mininko permits (Mali) and mineral resource estimate for the nampala gold mine. Robex Resour. Inc. 169.

Klemme, S., O'Neill, H.S., 2000. The near–solidus transition from garnet lherzolite to spinel lherzolite. Contrib. Miner. Petrol. 138 (3), 237–248.

Konate, S.I.M., Bolarinwa, A.T., Kwayisi, D., Kazapoe, R.W., Traore, E.M., Tcha, N.D.N., Kouagou, D., & Bouare, M.L. (2024). *Provenance and tectonic setting of greywacke and siltstone of the Nampala gold deposit, Southern Mali*. https://doi.org/10.1177/25726838241263698.

Kröner, A., Alexeiev, D.V., Rojas-Agramonte, Y., Hegner, E., Wong, J., Xia, X., Belousova, E., Mikolaichuk, A.V., Seltmann, R., Liu, D., Kiselev, V.V., 2013. Mesoproterozoic (Grenville-age) terranes in the Kyrgyz North Tianshan: Zircon ages and Nd–Hf isotopic constraints on the origin and evolution of basement blocks in the southern Central Asian Orogen. Gondwana Res. 23 (1), 272–295.

Lambert-Smith, J.S., Lawrence, D.M., Müller, W., Treloar, P.J., 2016. Palaeotectonic setting of the south-eastern Kédougou-Kéniéba Inlier, West Africa: New insights from igneous trace element geochemistry and U-Pb zircon ages. Precambrian Res. 274, 110–135. https://doi.org/10.1016/j.precamres.2015.10.013.

Li, C., Yan, J., 2021. Geochemical, mineralogy, and Sr–Nd–Pb isotopic compositions of the gold-related lamprophyre in the Bengbu–Wuhe Area, southeastern North China Craton: Implications for gold mineralization. Ore Geology Reviews 132, 104050.

Liégeois, J.P., Claessens, W., Camara, D., Klerkx, J., 1991. Short-lived eburnean orogeny in southern Mali. Geology, tectonics, U–Pb and Rb–Sr geochronology. Precambrian Res 50, 111–136.

Lonov, D.A., Griffin, W.L., O'Reilly, S.Y., 1997. Volatile–bearing minerals and lithophile trace elements in the upper mantle. Chem. Geol. 141 (3–4), 153–184.

Maniar, P.D., Piccoli, P.M., 1989. Tectonic discrimination of granitoids. Geological society of America bulletin 101 (5), 635–643.

Marchand, J., 2012. Form 43-101F1 technical evaluation report. Robex Resources Inc, p. 50.

Mcfarlane, C.R.M., Mavrogenes, J., Lentz, D., King, K., Allibone, A., Holcombe, R., 2011. Geology and intrusion-related affinity of the morila gold mine, Southeast Mali. Econ. Geol. 106 (5), 727–750. https://doi.org/10.2113/econgeo.106.5.727.

McFarlane, H.B., Ailleres, L., Betts, P., Ganne, J., Baratoux, L., Jessell, M.W., Block, S., 2019. Episodic collisional orogenesis and lower crust exhumation during the Palaeoproterozoic Eburnean Orogeny: evidence from the Sefwi Greenstone Belt, West African Craton. Precambrian Research 325, 88–110.

Middlemost, E.A., 1994. Naming materials in the magma/igneous rock system. Earth-science reviews 37 (3-4), 215–224.

O'connor, J.T., 1965. A classification for quartz-rich igneous rocks based on feldspar ratios. US Geological Survey Professional paper B 525, 79–84.

Olson, S.F., Diakité, K., Ott, L., Guindo, A., Forb, C.R.B., Winer, N., Hanssen, E., Lay, N., Bradley, R., Pohl, D., 1992. Proterozoic Syama Gold Deposit, Mali West Africa. Economic Geology 84, 310–331.

Palme, H., O'Neill, H.S., 2014. Cosmochemical estimates of mantle composition. Treatise on Geochemistry. Elsevier-Pergamon, *Oxford*, pp. 1–39.

Pearce, J.A., Harris, N.B., Tindle, A.G., 1984. Trace element discrimination diagrams for the tectonic interpretation of granitic rocks. Journal of petrology 25 (4), 956–983.

Rock, N.M.S., 1991. Thomson litho ltd, East Kilbride. Lamprophyres 1–285.

Rudnick, R.L., Fountain, D.M., 1995. Nature and composition of the continental crust: a lower crustal perspective. Rev. Geophys 33, 267–309.

Rudnick, R.L., Gao, S., 2003. The composition of the continental crust. In: Rudnick, R.L. (Ed.), In the Crust, Treatise on Geochemistry, 3. Elsevier, Oxford, pp. 1–64.

Rudnick, R.L., Gao, S., 2014. Composition of the Continental Crust. In: Holland, H.D., Turekian, K.K. (Eds.), Treatise on Geochemistry, 2nd ed. Elsevier-Pergamon, Oxford, pp. 1–51.

Sakyi, P.A., Anum, S., Su, B.X., Nude, P.M., Su, B.C., Asiedu, D.K., Nyame, F., Kwayisi, D., 2018. Geochemical and Sr-Nd isotopic records of Paleoproterozoic metavolcanics and mafic intrusive rocks from the West African Craton: evidence for petrogenesis and tectonic setting. Geol. J. 53 (2), 725–741.

Sakyi, P.A., Manu, J., Su, B.X., Kwayisi, D., Nude, P.M., Dampare, S.B., 2019. Geochemical and Sm–Nd isotopic evidence for the composition of the Palaeoproterozoic crust of the West African Craton in Ghana. Geol. J. 54 (6), 3940–3957.

Sakyi, P.A., Su, B.-X., Anum, S., Kwayisi, D., Dampare, S.B., Anani, C.Y., Nude, P.M., 2014. New zircon U–Pb ages for erratic emplacement of 2213–2130 Ma Paleoproterozoic calc-alkaline I-type granitoid rocks in the Lawra Volcanic Belt of Northwestern Ghana, West Africa. Precambrian Res. 254, 149–168.

Sakyi, P.A., Su, B.-X., Manu, J., Kwayisi, D., Anani, C.Y., Alemayehu, M., Malaviarachchi, S.P., Nude, P.M., Su, B.-C., 2020. Origin and tectonic significance of the metavolcanic rocks and mafic enclaves from the Palaeoproterozoic Birimian Terrane, SE West African Craton, Ghana. Geol. Mag. 157 (8), 1349–1366.

Salvi, S., Sangaré, A., Driouch, Y., Siebenaller, L., Béziat, D., Debat, P., Femenias, O., 2015. The Kalana vein-hosted gold deposit, southern Mali. Ore Geol. Rev. https://doi.org/10.1016/j.oregeorev.2015.10.011.

Sangare A. (2015). *Geology of Kalana Gold deposit (Southwest Mali), Petrogenesis, Metallogeny and Fluid inclusion study (Doctoral dissertation, University Sidi Mohamed Ben Abdellah, Morroco)*.

Senyah, G.A., Dampare, S.B., Asiedu, D.K., 2016. Geochemistry and tectonic setting of the Paleoproterozoic metavolcanic rocks from the Chirano Gold District, Sefwi belt, Ghana. J. Afr. Earth Sci. 122, 32–46.

Spandler, C., Pirard, C., 2013. Element recycling from subducting slabs to arc crust: a review. Lithos 208–223.

Stolz, A.J., Jochum, K.P., Spettel, B., Hofmann, A.W., 1996. Fluid-and melt-related enrichment in the subarc mantle: Evidence from Nb/Ta variations in island-arc basalts. Geology 24, 587–590.

Sun, S.S., McDonough, W.F., 1989. Chemical and isotopic systematics of oceanic basalts: implication for mantle composition and processes. In: Sauders, A.D., Norry, M.J. (Eds.), Magmatism in the Ocean Basins, Special Publication, 42. Geological Society, London, pp. 313–345.

Taylor, S.R., McLennan, S.M., 1985. The continental crust: its composition and evolution: An examination of the geochemical record preserved in sedimentary rocks. Blackwell Scientific Publications.

Traore D.Y. (2017). *Etude Metallogenique du district aurifere de Syama (Mali): Analyse comparative de gisements situés sur une meme structure lithosphériques éburnéenne, (Doctorat de l'Université* de *Toulouse*).

Traore, Y.D., Sanogo, S., Kone, A.Y., N'Diaye, I., Bouare, M.L., Beziat, D., 2022. Geochemistry of magmatic rocks of the syama belt, Southern Mali, West Africa Craton, 2022, 250–272. https://doi.org/10.4236/ojg.2022.123014.

Traoré, K., Chardon, D., Naba, S., Wane, O., Bouaré, M.L., 2022. Paleoproterozoic collision tectonics in West Africa: insights into the geodynamics of continental growth. Precambrian Res. 376 (February). https://doi.org/10.1016/j.precamres.2022.106692.

Wan, L., Zeng, Z., Kusky, T.M., Asimow, P.D., He, C., Liu, Y., Yang, S., Xu, S., 2019. Geochemistry of middle-late Mesozoic mafic intrusions in the eastern North China Craton: new insights on lithospheric thinning and decratonization. Gondwana Res 73, 153–174.

Wane O. (2010). *Etude géologique du Birimien de la région de Massigui (Paléoprotérozoïque du Mali méridional): la zone de cisaillement du Banifing, structure majeure du craton ouest africain*. These, Université de Lille 1.

Wane, O., Liégeois, J.P., Thébaud, N., Miller, J., Metelka, V., Jessell, M., 2018. The onset of the Eburnean collision with the Kenema-Man craton evidenced by plutonic and volcanosedimentary rock record of the Masssigui region, southern Mali. Precambrian Res. 444–478. https://doi.org/10.1016/j.precamres.2017.11.008.

Wang, Y., Fan, W., Sun, M., Liang, X., Zhang, Y., Peng, T., 2007. Geochronological, geochemical and geothermal constraints on petrogenesis of the Indosinian peraluminous granites in the South China Block: a case study in the Hunan Province. Lithos 96 (3-4), 475–502.

Wilson, M. (Ed.), 1989. Igneous petrogenesis. Springer, Netherlands.

Winter, J.D. (2001). An introduction to igneous and metamorphic petrology.